The Journal of Chemical Physics

RESEARCH ARTICLE | NOVEMBER 08 2023

Exact two-component theory becoming an efficient tool for NMR shieldings and shifts with spin–orbit coupling

Special Collection: 2023 JCP Emerging Investigators Special Collection

Yannick J. Franzke ; Christof Holzer

J. Chem. Phys. 159, 184102 (2023)
https://doi.org/10.1063/5.0171509

The Journal of Chemical Physics ARTICLE pubs.aip.org/aip/jcp

Exact two-component theory becoming an efficient tool for NMR shieldings and shifts with spin–orbit coupling

Cite as: J. Chem. Phys. 159, 184102 (2023); doi: 10.1063/5.0171509
Submitted: 9 August 2023 • Accepted: 4 September 2023 •
Published Online: 8 November 2023

Yannick J. Franzke[1,a] and Christof Holzer[2,a]

AFFILIATIONS

[1] Fachbereich Chemie, Philipps–Universität Marburg, Hans-Meerwein-Straße 4, 35032 Marburg, Germany
[2] Institute of Theoretical Solid State Physics, Karlsruhe Institute of Technology (KIT), Wolfgang-Gaede-Straße 1, 76131 Karlsruhe, Germany

Note: This paper is part of the 2023 JCP Emerging Investigators Special Collection.
[a] **Authors to whom correspondence should be addressed:** yannick.franzke@chemie.uni-marburg.de and christof.holzer@kit.edu

ABSTRACT

We present a gauge-origin invariant exact two-component (X2C) approach within a modern density functional framework, supporting meta-generalized gradient approximations such as TPSS and range-separated hybrid functionals such as CAM-B3LYP. The complete exchange-correlation kernel is applied, including the direct contribution of the field-dependent basis functions and the reorthonormalization contribution from the perturbed overlap matrix. Additionally, the finite nucleus model is available for the electron-nucleus potential and the vector potential throughout. Efficiency is ensured by the diagonal local approximation to the unitary decoupling transformation in X2C as well as the (multipole-accelerated) resolution of the identity approximation for the Coulomb term (MARI-J, RI-J) and the seminumerical exchange approximation. Errors introduced by these approximations are assessed and found to be clearly negligible. The applicability of our implementation to large-scale calculations is demonstrated for a tin pincer-type system as well as low-valent tin and lead complexes. Here, the calculation of the Sn nuclear magnetic resonance shifts for the pincer-type ligand with about 2400 basis functions requires less than 1 h for hybrid density functionals. Further, the impact of spin–orbit coupling on the nucleus-independent chemical shifts and the corresponding ring currents of all-metal aromatic systems is studied.

I. INTRODUCTION

Determining nuclear magnetic resonance (NMR) parameters is a widespread tool in the structural and conformational analysis of molecular systems. The theoretical approaches for the calculation of these parameters using *ab initio* quantum mechanical methods accordingly evolved quickly.[1–3] While initially theory focused on non-relativistic (NR) methods, NMR parameters are of course heavily affected by the behavior of the core electrons. Already for moderately heavy nuclei with an atomic number $Z > 18$, neglecting relativistic effects will consequently start to severely deteriorate the obtained NMR parameters.[4–8] Relativistic quantum mechanical ansätze such as the zeroth-order regular approximation (ZORA),[9–11] (one-electron) exact two-component (X2C) theory,[12–18] or fully relativistic Dirac–Coulomb (DC) methods[19,20] therefore readily emerged for these parameters, given their high importance in calculations that involve electrons near the nucleus. For instance, fully relativistic four-component (4c) approaches with the Dirac–Coulomb Hamiltonian to compute NMR shieldings were presented in Refs. 21–30. In contrast to the non-relativistic formalism, not only the use of gauge-including atomic orbitals (GIAOs) or London atomic orbitals[31,32] but also a magnetic balance condition are required. The latter is of crucial importance for the diamagnetic terms and can be included either with the restricted magnetic balance[21,22] (RMB) or the simple magnetic balance (sMB) scheme.[28,29] The RMB-GIAO formalism was later

applied to scalar one-component (1c) or spin-free X2C[33,34] and two-component (2c) spin–orbit (SO) X2C approaches.[35,36] Note that the corresponding spin–orbit X2C ansatz was so far only combined with Hartree–Fock (HF) theory. Other X2C formulations have been presented in Refs. 37 and 38. So far, most and in particular large-scale spin–orbit studies are typically carried out with the formally inferior ZORA ansatz,[39–41] see for instance the studies in Refs. 42–50.

The drawback of all these 2c and 4c methods is twofold. On the one hand, the computational demands are steeply increased compared to non- and scalar-relativistic (SR) approaches to the calculation of NMR parameters. While 2c approaches already provide a distinct advantage over four-component calculations concerning the wall times for the determination of NMR parameters, still such calculations remain tedious. This severely hampers the routine theoretical assessment of NMR parameters for sizable molecular systems with more than 50–60 atoms. Yet, 2c approaches have proven to be good trade offs, as the loss in accuracy is often minimal, equaling only a few percent at maximum as will be demonstrated for NMR shielding constants. Likely, for chemical shifts even lower errors can be expected due to error cancellation, given that only relative values are needed for the latter. Especially when paired with density functional theory (DFT), the difference between 4c and 2c results becomes negligible when compared to the variation for NMR parameters between different density functional approximations.[42,51–54] On the other hand, especially in the framework of DFT, also the formulation of the coupled-perturbed Kohn–Sham (CPKS) equations including spin–orbit coupling becomes increasingly difficult. This has hampered 2c and 4c implementations for density functionals that depend on the kinetic-energy density, as for example many meta-generalized gradient approximations (meta-GGAs). Relativistic NMR studies were therefore cut off from many functionals known to perform well for the prediction of NMR parameters of lighter elements.[42,54]

This paper aims at alleviating these drawbacks. First, an efficient yet accurate scheme for generally obtaining 2c NMR shieldings and shifts is outlined. To achieve optimal efficiency, state-of-the-art techniques such as the resolution of the identity (RI) approximation[55–57] and the seminumerical integral evaluation[58–63] are adapted and combined with the efficient X2C technique. Especially exploiting the locality of the relativistic X2C transformation can yield further speedups.[34] Second, the necessary adaptions to take into account the kinetic-energy density will be discussed. Combined, the new developments will allow for an accurate description of NMR shieldings and shift, taking into account relativistic effects. The errors of the implemented spin–orbit X2C-DFT approach will be assessed using fully relativistic 4c reference values. Furthermore, the performance and reliability of the seminumerical and RI approximation will be tested for NMR quantities.

II. THEORY

A. NMR shielding tensor for Kramers-restricted systems

The NMR shielding tensor σ^I_{uw} $(u, w = x, y, z)$ of a nucleus I is given as the derivative of the energy E with respect to the external magnetic field $\vec{B}$ and the nuclear magnetic moment $\vec{m}_I$

$$\sigma^I_{wu} = \frac{\partial^2 E}{\partial B_u \partial m_{I,w}} = \mathrm{tr}\left(\mathbf{P}\frac{\partial^2 \mathbf{h}}{\partial B_u \partial m_{I,w}}\right) + \mathrm{tr}\left(\frac{\partial \mathbf{P}}{\partial B_u}\frac{\partial \mathbf{h}}{\partial m_{I,w}}\right). \quad (1)$$

Here, $\mathbf{P}$ denotes the one-electron density matrix and $\mathbf{h}$ the one-electron Hamiltonian. Note that derivatives are formed in the limit of a vanishing perturbation, i.e., in the limit of vanishing $\vec{B}$ and $\vec{m}_I$. These magnetic perturbations are introduced with the principle of minimal coupling[64]

$$\hat{\vec{p}} \to \hat{\vec{\pi}} = \hat{\vec{p}} + \frac{1}{c}\hat{\vec{A}}_O = \hat{\vec{p}} + \frac{1}{c}\hat{\vec{A}}^B_O + \frac{1}{c}\sum_I \hat{\vec{A}}^m_I \quad (2)$$

which generalizes the momentum operator $\hat{p}$ with the vector potential $\vec{A}$ of the external magnetic field and the nuclear magnetic moments,

$$\vec{A}^B_O(\vec{r}) = \frac{1}{2}\vec{B} \times \vec{r}_O \quad \vec{r}_O = \vec{r} - \vec{R}_O, \quad (3)$$

$$\vec{A}^m_I(\vec{r}) = -\vec{m}_I \times \vec{\nabla} G_I(\vec{r}), \quad G_I(\vec{r}) = \int \frac{w_I(\vec{R}_I)}{|\vec{r} - \vec{R}|} d\vec{R}, \quad (4)$$

$$w_I(\vec{R}_I) = \left(\frac{\zeta}{\pi}\right)^{3/2} \exp\left(-\zeta(\vec{R} - \vec{R}_I)^2\right). \quad (5)$$

Here, $\vec{R}_O$ is the gauge origin and w_I is the shape function of the nuclear charge distribution,[65,66] which is approximated as a Gaussian function with the exponent ζ in this work.[67] Uppercase and lowercase letters refer to nuclear and electronic coordinates, respectively. c is the speed of light.

The one-electron density matrix $\mathbf{P}$ in the two-component formalism reads

$$\mathbf{P} = \begin{pmatrix} \boldsymbol{P}^{\alpha\alpha} & \boldsymbol{P}^{\alpha\beta} \\ \boldsymbol{P}^{\beta\alpha} & \boldsymbol{P}^{\beta\beta} \end{pmatrix} \quad (6)$$

with the one-component spin density matrices

$$\mathrm{Re}(\boldsymbol{P}^{\sigma\sigma'}_{\mu\nu}) = \sum_i n_i \left[\mathrm{Re}(c^{\sigma}_{\mu i})\mathrm{Re}(c^{\sigma'}_{\nu i}) + \mathrm{Im}(c^{\sigma}_{\mu i})\mathrm{Im}(c^{\sigma'}_{\nu i})\right] \quad (7)$$

$$\mathrm{Im}(\boldsymbol{P}^{\sigma\sigma'}_{\mu\nu}) = \sum_i n_i \left[-\mathrm{Im}(c^{\sigma}_{\mu i})\mathrm{Re}(c^{\sigma'}_{\nu i}) + \mathrm{Re}(c^{\sigma}_{\mu i})\mathrm{Im}(c^{\sigma'}_{\nu i})\right] \quad (8)$$

which are evaluated with the occupation numbers n_i of the corresponding two-component spinor states associated with the energy eigenvalues ε_i and the self-consistent field (SCF) coefficients $\{c_{\mu i}\}$. μ, ν denote the one-electron basis functions and the superscript σ the spin component $(\sigma = \alpha, \beta)$. Bold letters indicate a two-component matrix, while italic bold letters refer to the one-component space. For a closed-shell Kramers-restricted system, only the symmetric total density matrix

$$D^0_{\mu\nu} = \mathrm{Re}(D^{\alpha\alpha}_{\mu\nu}) + \mathrm{Re}(D^{\beta\beta}_{\mu\nu}) \quad (9)$$

as well as the three antisymmetric spin-density matrices

$$D^x_{\mu\nu} = \mathrm{Im}(D^{\alpha\beta}_{\mu\nu}) + \mathrm{Im}(D^{\beta\alpha}_{\mu\nu}), \quad (10)$$

$$D^y_{\mu\nu} = \mathrm{Re}(D^{\beta\alpha}_{\mu\nu}) - \mathrm{Re}(D^{\alpha\beta}_{\mu\nu}), \quad (11)$$

$$D^{z}_{\mu\nu} = \mathrm{Im}(D^{\alpha\alpha}_{\mu\nu}) - \mathrm{Im}(D^{\beta\beta}_{\mu\nu}) \tag{12}$$

are non-zero without external perturbations. The latter three are associated with the spin-current density induced by spin–orbit coupling. See, for instance, Ref. 68. Note that an external perturbation such as a magnetic field gives rise to the imaginary and antisymmetric counter part of the total density matrix via response equations[32,69,70] and similarly for the spin density matrices.[22,29]

We will first briefly describe the unperturbed density contribution to the NMR shielding tensor with the DLU-X2C Hamiltonian and then discuss the perturbed density contribution, which requires to solve the coupled-perturbed Hartree–Fock (CPHF) or coupled-perturbed Kohn–Sham equations.[71–75]

B. Unperturbed density contribution

The first term of Eq. (1) necessitates the second derivative of the X2C/DLU-X2C Hamiltonian. Detailed discussions of analytical derivatives in the X2C and DLU-X2C formalism can be found in the literature[33–36,76–90] so that we just state the working equations for the NMR shieldings in DLU-X2C. This means that the work of Ref. 34 is generalized to the two-component formalism. Note that the first-order X2C/DLU-X2C derivatives in the RMB-GIAO formalism for the shielding tensor are the same as those for the NMR spin–spin coupling constants[83–85] or electron paramagnetic resonance (EPR) g-tensors,[91] as the vector potential associated with the nuclear magnetic moments is commonly neglected in the RMB condition for X2C NMR properties.[33–36,83,84] Herein, we use the one-electron X2C ansatz and account for the missing two-electron integrals in the X2C transformation with the (modified) screened nuclear spin–orbit (SNSO/mSNSO) approximation.[80,92,93] Comparison of X2C and 4c Dirac–Kohn–Sham results for NMR coupling constants, the electron paramagnetic resonance (EPR) hyperfine coupling constant as well as the EPR and g-tensor have shown that the mSNSO approximation yields excellent results and does not increase the computational demands.[84,91,94,95]

The mixed second-order derivative in the RMB-GIAO formalism read

$$\begin{aligned}\mathbf{h}^{B,m} = {}& \mathbf{R}^{\dagger,B,m}\,\mathbf{L}\,\mathbf{R} + \mathbf{R}^{\dagger}\,\mathbf{L}\,\mathbf{R}^{B,m} + \mathbf{R}^{\dagger}\,\mathbf{L}^{B,m}\,\mathbf{R} \\ & + \mathbf{R}^{\dagger,B}\,\mathbf{L}\,\mathbf{R}^{m} + \mathbf{R}^{\dagger,m}\,\mathbf{L}\,\mathbf{R}^{B} + \mathbf{R}^{\dagger,B}\,\mathbf{L}^{m}\,\mathbf{R} \\ & + \mathbf{R}^{\dagger}\,\mathbf{L}^{m}\,\mathbf{R}^{B} + \mathbf{R}^{\dagger,m}\,\mathbf{L}^{B}\,\mathbf{R} + \mathbf{R}^{\dagger}\,\mathbf{L}^{B}\,\mathbf{R}^{m}.\end{aligned} \tag{13}$$

For brevity, we dropped the indices for the Cartesian components or the specific nucleus. Additionally, we use a short-hand notation (superscripts) to indicate the derivatives (B, m). Here, the renormalization matrix $\mathbf{R}$ reads[18]

$$\mathbf{R} = \mathbf{S}^{-1/2}\left(\mathbf{S}^{-1/2}\tilde{\mathbf{S}}\mathbf{S}^{-1/2}\right)^{-1/2}\mathbf{S}^{1/2}, \tag{14}$$

$$\tilde{\mathbf{S}} = \mathbf{S} + \frac{1}{2c^2}\mathbf{X}^{\dagger}\mathbf{T}\mathbf{X}, \tag{15}$$

$$\mathbf{X} = \mathbf{C}^{\mathrm{S}}_{+}(\mathbf{C}^{\mathrm{L}}_{+})^{-1}, \tag{16}$$

which necessitates the decoupling matrix $\mathbf{X}$ constructed with the large (L) and small (S) component eigenvectors of the so-called electronic states (+) from a diagonalization of the one-electron Dirac matrix.[12–18] Here, $\mathbf{S}$ and $\mathbf{T}$ are the overlap and kinetic-energy matrix

$$\mathbf{S} = \begin{pmatrix} \boldsymbol{S} & 0 \\ 0 & \boldsymbol{S} \end{pmatrix}, \quad \boldsymbol{S}_{\mu\nu} = \langle\chi_\mu|\chi_\nu\rangle, \tag{17}$$

$$\mathbf{T} = \begin{pmatrix} \boldsymbol{T} & 0 \\ 0 & \boldsymbol{T} \end{pmatrix}, \quad \boldsymbol{T}_{\mu\nu} = -\left\langle\chi_\mu\left|\frac{\hat{p}^2}{2}\right|\chi_\nu\right\rangle \tag{18}$$

in atomic units. For clarity, χ_μ is a one-component basis function and ϕ_μ a two-component function given as a direct product of a spatial 1c function and the spin function.[96] We refer to the literature for the derivatives of $\mathbf{R}$ based on Sylvester matrix equations.[79] For completeness, see Appendix A.

$\mathbf{L}$ is originally known from the normalized elimination of the small component (NESC) ansatz[97–101] and the unperturbed NESC matrix reads

$$\mathbf{L} = \mathbf{V} + \mathbf{X}^{\dagger}\mathbf{T} + \mathbf{T}\mathbf{X} + \mathbf{X}^{\dagger}\left(\frac{1}{4c^2}\mathbf{W} - \mathbf{T}\right)\mathbf{X} \tag{19}$$

with the potential $\mathbf{V}$ and the relativistically modified potential matrix defined according to $\mathbf{W}$

$$\mathbf{V} = \begin{pmatrix} \boldsymbol{V} & 0 \\ 0 & \boldsymbol{V} \end{pmatrix}, \quad \boldsymbol{V}_{\mu\nu} = \langle\chi_\mu|\hat{V}|\chi_\nu\rangle, \tag{20}$$

$$\mathbf{W}_{\mu\nu} = \left\langle\phi_\mu\left|\left(\vec{\sigma}\cdot\hat{\vec{p}}\right)\hat{V}\left(\vec{\sigma}\cdot\hat{\vec{p}}\right)\right|\phi_\nu\right\rangle. \tag{21}$$

Herein, we use the electron-nucleus potential operator $\hat{V}$ in the finite nucleus model with a Gaussian charge distribution.[67] The three Pauli spin matrices σ_u $(u = x, y, z)$ are collected in the vector $\vec{\sigma}$.

The first-order derivatives of the NESC matrix are given as

$$\begin{aligned}\mathbf{L}^{B} = {}& \mathbf{V}^{B} + \mathbf{\Pi}^{\dagger,B}\,\mathbf{X} + \mathbf{T}\,\mathbf{X}^{B} + \mathbf{X}^{\dagger,B}\,\mathbf{T} + \mathbf{X}^{\dagger}\,\mathbf{\Pi}^{B} \\ & + \mathbf{X}^{\dagger,B}\left(\frac{1}{4c^2}\mathbf{W} - \mathbf{T}\right)\mathbf{X} + \mathbf{X}^{\dagger}\left(\frac{1}{4c^2}\mathbf{W}^{B} - \mathbf{T}^{B}\right)\mathbf{X} \\ & + \mathbf{X}^{\dagger}\left(\frac{1}{4c^2}\mathbf{W} - \mathbf{T}\right)\mathbf{X}^{B}\end{aligned} \tag{22}$$

and

$$\begin{aligned}\mathbf{L}^{m} = {}& \mathbf{\Pi}^{\dagger,m}\,\mathbf{X} + \mathbf{T}\,\mathbf{X}^{m} + \mathbf{X}^{\dagger,m}\,\mathbf{T} + \mathbf{X}^{\dagger}\,\mathbf{\Pi}^{m} \\ & + \mathbf{X}^{\dagger,m}\left(\frac{1}{4c^2}\mathbf{W} - \mathbf{T}\right)\mathbf{X} + \mathbf{X}^{\dagger}\left(\frac{1}{4c^2}\mathbf{W} - \mathbf{T}\right)\mathbf{X}^{m}.\end{aligned} \tag{23}$$

Additionally, the second derivative of the NESC matrix is given as

$$\begin{aligned}\mathbf{L}^{B,m} = {}& \mathbf{\Pi}^{\dagger,B,m}\,\mathbf{X} + \mathbf{\Pi}^{\dagger,B}\,\mathbf{X}^{m} + \mathbf{\Pi}^{\dagger,m}\,\mathbf{X}^{B} + \mathbf{T}\,\mathbf{X}^{B,m} \\ & + \mathbf{X}^{\dagger,B,m}\,\mathbf{T} + \mathbf{X}^{\dagger,B}\,\mathbf{\Pi}^{m} + \mathbf{X}^{\dagger,m}\,\mathbf{\Pi}^{B} + \mathbf{X}^{\dagger}\,\mathbf{\Pi}^{B,m} \\ & + \mathbf{X}^{\dagger,B,m}(\mathbf{W} - \mathbf{T})\mathbf{X} + \mathbf{X}^{\dagger,m}\left(\mathbf{W}^{B} - \mathbf{T}^{B}\right)\mathbf{X} \\ & + \mathbf{X}^{\dagger,B}(\mathbf{W} - \mathbf{T})\mathbf{X}^{m} + \mathbf{X}^{\dagger,m}(\mathbf{W} - \mathbf{T})\mathbf{X}^{B} \\ & + \mathbf{X}^{\dagger}\left(\mathbf{W}^{B} - \mathbf{T}^{B}\right)\mathbf{X}^{m} + \mathbf{X}^{\dagger}(\mathbf{W} - \mathbf{T})\mathbf{X}^{B,m}.\end{aligned} \tag{24}$$

In the finite nucleus model, the one-electron derivatives for the magnetic field read as follows.[91] The potential and overlap matrix are the same as in the non-relativistic limit

$$\mathbf{V}^{B_u}_{\mu\nu} = \frac{\mathrm{i}}{2c}\sigma_0\left\langle\chi_\mu\middle|(\vec{R}_{\mu\nu}\times\hat{\vec{r}})_u\ \hat{V}\middle|\chi_\nu\right\rangle, \tag{25}$$

$$\mathbf{S}^{B_u}_{\mu\nu} = \frac{\mathrm{i}}{2c}\sigma_0\left\langle\chi_\mu\middle|(\vec{R}_{\mu\nu}\times\hat{\vec{r}})_u\middle|\chi_\nu\right\rangle. \tag{26}$$

σ_0 denotes the (2×2) identity matrix. Note that the derivative $\mathbf{S}^{B_u}_{\mu\nu}$ is needed for the respective derivative of the renormalization matrix $\mathbf{R}$, see Appendix A. These derivatives only arise through the GIAOs[31,32]

$$\chi_\mu\left(\vec{B},\vec{r}\right) = \exp\left(-\mathrm{i}\Lambda_{\mu O}\right)\chi_\mu(\vec{r}), \tag{27}$$

$$\Lambda_{\mu O}\left(\vec{B},\vec{r}\right) = \frac{1}{2c}(\vec{R}_{\mu O}\times\vec{r})\cdot\vec{B}. \tag{28}$$

Further, the corresponding derivative of the kinetic-energy matrix follows as

$$\begin{aligned}\mathbf{T}^{B_u}_{\mu\nu} = {}& \frac{\mathrm{i}}{4c}\sigma_0\left\langle\chi_\mu\middle|(\vec{R}_{\mu\nu}\times\hat{\vec{r}})_u\ \hat{\vec{p}}^{\,2}\middle|\chi_\nu\right\rangle \\ & + \frac{1}{2c}\sigma_0\left\langle\chi_\mu\middle|(\hat{\vec{r}}_\nu\times\hat{\vec{p}})_u\middle|\chi_\nu\right\rangle + \frac{1}{2c}\sigma_u\langle\chi_\mu|\chi_\nu\rangle\end{aligned} \tag{29}$$

with $\vec{r}_\nu$ denoting the electronic position vector relative to the atom center of the basis function χ_ν. The generalized momentum contribution is

$$\begin{aligned}\mathbf{\Pi}^{\dagger,B_u}_{\mu\nu} = {}& \frac{\mathrm{i}}{4c}\sigma_0\left\langle\chi_\mu\middle|(\vec{R}_{\mu\nu}\times\hat{\vec{r}})_u\ \hat{\vec{p}}^{\,2}\middle|\chi_\nu\right\rangle \\ & + \frac{1}{2c}\sigma_0\left\langle\chi_\mu\middle|(\hat{\vec{r}}_\nu\times\hat{\vec{p}})_u\middle|\chi_\nu\right\rangle + \frac{1}{2c}\sigma_u\langle\chi_\mu|\chi_\nu\rangle.\end{aligned} \tag{30}$$

Finally, the derivative of the relativistically modified potential matrix is given as

$$\begin{aligned}\mathbf{W}^{B_u}_{\mu\nu} = {}& \frac{\mathrm{i}}{2c}\sigma_0\left\langle\chi_\mu\middle|(\vec{R}_{\mu\nu}\times\hat{\vec{r}})_u\ \hat{\vec{p}}\cdot\hat{V}\hat{\vec{p}}\middle|\chi_\nu\right\rangle \\ & + \frac{1}{2c}\sigma_0\left\langle\chi_\mu\middle|(\hat{\vec{r}}_\nu\times\hat{\vec{p}})_u\ \hat{V} + \hat{V}\ (\hat{\vec{r}}_\nu\times\hat{\vec{p}})_u\middle|\chi_\nu\right\rangle \\ & + \frac{1}{2c}\left\langle\chi_\mu\middle|(\vec{R}_{\mu\nu}\times\hat{\vec{r}})_u\ \ \mathrm{i}\vec{\sigma}\cdot\left(\hat{\vec{p}}\times\hat{V}\hat{\vec{p}}\right)\middle|\chi_\nu\right\rangle \\ & + \left\langle\chi_\mu\middle|\frac{\mathrm{i}}{2c}\sigma_u\left(\hat{\vec{p}}\ \hat{V}\right)\cdot\hat{\vec{r}}_\nu - \frac{\mathrm{i}}{2c}\left(\hat{\vec{p}}\ \hat{V}\right)_u(\vec{\sigma}\cdot\hat{\vec{r}}_\nu)\middle|\chi_\nu\right\rangle \\ & + \frac{1}{c}\sigma_u\langle\chi_\mu|\hat{V}|\chi_\nu\rangle.\end{aligned} \tag{31}$$

For the derivatives with respect to the magnetic moment, only the generalized momentum matrix is non-zero and reads[84]

$$\begin{aligned}\mathbf{\Pi}^{\dagger,m_{I,w}}_{\mu\nu} = {}& \frac{1}{2c}\left\langle\phi_\mu\middle|\left(\vec{\nabla}_I\hat{G}_I\times\vec{\sigma}\right)_w\middle|\left(\vec{\sigma}\cdot\hat{\vec{p}}\right)\phi_\nu\right\rangle \\ = {}& \frac{1}{2c}\sigma_0\left\langle\chi_\mu\middle|\left(\vec{\nabla}_I\hat{G}_I\times\hat{\vec{p}}\right)_w\middle|\chi_\nu\right\rangle \\ & + \frac{\mathrm{i}}{2c}\left\langle\chi_\mu\middle|\left(\left[\vec{\sigma}\cdot\vec{\nabla}_I\hat{G}_I\right]\hat{p}_w - \sigma_w\left[\vec{\nabla}_I\hat{G}_I\cdot\hat{\vec{p}}\right]\right)\middle|\chi_\nu\right\rangle.\end{aligned} \tag{32}$$

Here, we partitioned the integral into the scalar and the spin–orbit contribution. $\mathbf{\Pi}^{m_{I,w}}_{\mu\nu}$ is defined accordingly.

The spin-free or scalar-relativistic (SR) contribution to the mixed second derivatives is[34]

$$\begin{aligned}\mathbf{\Pi}^{\dagger,B_u m_{I,w}}_{\mu\nu,SR} = {}& \sigma_0\frac{1}{4c^2}\left\langle\chi_\mu\middle|\delta_{uw}\left(\left[\vec{\nabla}_I\hat{G}_I\right]\cdot\hat{\vec{r}}_\nu\right) - \left[\vec{\nabla}_I\hat{G}_I\right]_u(\hat{\vec{r}}_\nu)_w\middle|\chi_\nu\right\rangle \\ & + \sigma_0\frac{\mathrm{i}}{4c^2}\left\langle\chi_\mu\middle|(\vec{R}_{\mu\nu}\times\hat{\vec{r}})_u\left(\left[\vec{\nabla}_I\hat{G}_I\right]\times\hat{\vec{p}}\right)_w\middle|\chi_\nu\right\rangle\end{aligned} \tag{33}$$

and the spin-dependent or spin–orbit (SO) contribution reads[102]

$$\begin{aligned}\mathbf{\Pi}^{\dagger,B_u m_{I,w}}_{\mu\nu,SO} = {}& -\frac{1}{2c^2}\left\langle\chi_\mu\middle|\left(\vec{R}_{\mu\nu}\times\hat{\vec{r}}\right)_u\vec{\sigma}\cdot\left[\vec{\nabla}_I\hat{G}_I\right]\hat{p}_w\middle|\chi_\nu\right\rangle \\ & + \frac{1}{2c^2}\left\langle\chi_\mu\middle|\left(\vec{R}_{\mu\nu}\times\hat{\vec{r}}\right)_u\sigma_w\left[\vec{\nabla}_I\hat{G}_I\right]\cdot\hat{\vec{p}}\middle|\chi_\nu\right\rangle \\ & - \frac{\mathrm{i}}{4c^2}\left\langle\chi_\mu\middle|\varepsilon_{wua}\ \vec{\sigma}\cdot\left[\vec{\nabla}_I\hat{G}_I\right]\ (\hat{\vec{r}}_\nu)_w\middle|\chi_\nu\right\rangle \\ & + \frac{\mathrm{i}}{4c^2}\left\langle\chi_\mu\middle|\sigma_w\left(\hat{\vec{r}}_\nu\times\vec{\nabla}_I\hat{G}_I\right)_u\middle|\chi_\nu\right\rangle\end{aligned} \tag{34}$$

with the Kronecker delta δ_{uw} and Levi–Civita tensor ε_{wua}. See Ref. 33 for the corresponding expression in the point charge model of the scalar potential and the vector potential.

The only missing ingredients for Eq. (24) are the derivatives of the decoupling matrix $\mathbf{X}$. These are obtained by solving one-electron response equations similar to the CPHF/CPKS formalism.[76–79] However, no iterative procedure is required. We refer to the appendix of Ref. 34 for a detailed discussion. For completeness, we list the equations in the Appendix B. Note that complex algebra is needed for the 2c approach, while the scalar ansätze[33,34] can be implemented with real algebra only. Thus, the computational costs of the 2c ansatz rise due to the increased dimension and the use of complex algebra. Consequently, local approximations are desirable for large-scale applications.[103]

In DLU, the X2C response equations for $\mathbf{X}$ and the Sylvester matrix equations for $\mathbf{R}$ only need to be solved for the atomic diagonal blocks and the derivative of the Hamiltonian reads

$$\begin{aligned}\mathbf{h}^{B,m}_{AB} = {}& \mathbf{R}^{\dagger,B,m}_{AA}\ \mathbf{L}_{AB}\ \mathbf{R}_{BB} + \mathbf{R}^{\dagger}_{AA}\ \mathbf{L}_{AB}\ \mathbf{R}^{B,m}_{BB} + \mathbf{R}^{\dagger}_{AA}\ \mathbf{L}^{B,m}_{AB}\mathbf{R}_{BB} \\ & + \mathbf{R}^{\dagger,B}_{AA}\ \mathbf{L}_{AB}\ \mathbf{R}^{m}_{BB} + \mathbf{R}^{\dagger,m}_{AA}\ \mathbf{L}_{AB}\ \mathbf{R}^{B}_{BB} + \mathbf{R}^{\dagger,B}_{AA}\mathbf{L}^{m}_{AB}\ \mathbf{R}_{BB} \\ & + \mathbf{R}^{\dagger}_{AA}\ \mathbf{L}^{m}_{AB}\ \mathbf{R}^{B}_{BB} + \mathbf{R}^{\dagger,m}_{AA}\ \mathbf{L}^{B}_{AB}\ \mathbf{R}_{BB} + \mathbf{R}^{\dagger}_{AA}\ \mathbf{L}^{B}_{AB}\ \mathbf{R}^{m}_{BB}.\end{aligned} \tag{35}$$

where A, B refer to the atomic blocks defined with the atom center of the *bra* and *ket* basis function.[81,96,104] The atomic off-diagonal blocks of the NESC matrix are given by[81,96,104]

$$\mathbf{L}_{AB} = \mathbf{V}_{AB} + \mathbf{X}^{\dagger}_{AA}\ \mathbf{T}_{AB} + \mathbf{T}_{AB}\ \mathbf{X}_{BB} + \mathbf{X}^{\dagger}_{AA}\left(\frac{1}{4c^2}\mathbf{W}_{AB} - \mathbf{T}_{AB}\right)\mathbf{X}_{BB} \tag{36}$$

and the derivatives follow accordingly. The atomic off-diagonal blocks, AB, of the Hamiltonian derivatives are constructed from these diagonal blocks and the atomic off-diagonal blocks of the one-electron integrals and integral derivatives.[34,81]

C. Perturbed density contribution

The second term on the RHS of Eq. (1) contains the explicit derivative of the density matrix with respect to the external magnetic fields. It is therefore usually referred to as the perturbed

density contribution. The magnetic-field perturbed density contribution can be obtained in a similar manner to four-component DFT implementations for NMR shieldings.[28,29]

In the spirit of Ref. 105, the corresponding contribution of Eq. (1) is first recast into an explicit matrix form,

$$\mathrm{tr}\left(\frac{\partial \mathbf{P}}{\partial B_u}\frac{\partial \mathbf{h}}{\partial m_{I,w}}\right) = \sum_{\mu\nu}\frac{\partial \mathbf{h}_{\mu\nu}}{\partial m_{I,w}}\left(U^{B_u}_{\mu\nu} + V^{B_u}_{\mu\nu}\right), \tag{37}$$

The occupied-virtual part of $\{\mathbf{U}^{B_u}, \mathbf{V}^{B_u}\}$ in Eq. (37) are the solutions of the coupled perturbed Kohn–Sham equation

$$\begin{pmatrix}\mathbf{A} & \mathbf{B}\\ \mathbf{B}^* & \mathbf{A}^*\end{pmatrix}\begin{pmatrix}\mathbf{U}^B\\ \mathbf{V}^B\end{pmatrix} = \begin{pmatrix}\mathbf{P}^B\\ \mathbf{Q}^B\end{pmatrix} \tag{38}$$

with $\mathbf{Q}^B = \mathbf{P}^{*,B}$. The orbital rotation matrix on the left hand side of Eq. (38) is defined as usual

$$A_{ai,bj} = (\varepsilon_a - \varepsilon_i)\delta_{ij}\delta_{ab} + C_{ai,jb} \tag{39}$$

$$B_{ai,bj} = C_{ai,bj} \tag{40}$$

where $\mathbf{C}$ denotes the interaction kernel,

$$C_{pq,rs} = (pq|rs) + f^{\mathrm{XC}}_{pq,rs} - c_{\mathrm{X}}(ps|qr)\,. \tag{41}$$

$\mathbf{f}^{\mathrm{XC}}$ denotes the non-collinear exchange-correlation (XC) kernel[106–108] and $(pq|rs)$ is a complex 4-index electron repulsion integral in Mulliken notation. $i,j,\ldots$ denotes occupied spinor states and $a,b,\ldots$ refers to unoccupied or virtual spinors states. $p,q,\ldots$ are used for arbitrary spinors states. c_{X} describes the admixture of HF exchange for hybrid functionals. The right hand side, $\{\mathbf{P}^B, \mathbf{Q}^B\}$, then collects the perturbation contributions. When spin–orbit coupling is present, the perturbation contributions can be decomposed into two types and the overlap contribution

$$\mathbf{P}^B_{ai} = \mathbf{P}^1_{ai} + \mathbf{P}^2_{ai} - \boldsymbol{\varepsilon}_i \mathbf{S}^B_{ai}\,. \tag{42}$$

In this work, the common symmetric connection is used instead of the natural connection for the CPHF/CPKS formalism, cf. Ref. 28.

The first contribution solely arises from the differentiation of the introduced GIAO phase factor with respect to the magnetic field. It is obtained directly from the ground-state density as

$$\begin{aligned}\left[\boldsymbol{P}^{1,m}_{\mu\nu}\right]_u = &\sum_{\kappa\lambda} D^m_{\kappa\lambda}\left[\delta_{m0}\; J^{B_u}_{\mu\nu,\kappa\lambda} - c_{\mathrm{X}}\frac{1}{2}K^{B_u}_{\mu\nu,\kappa\lambda}\right]\\
&+ \delta_{m0}\frac{\mathrm{i}}{2c}\int\frac{\partial e^{\mathrm{XC}}}{\partial\rho_\uparrow(\vec{r})}(\vec{R}_{\mu\nu}\times\vec{r})_u\;\chi_\mu\chi_\nu\;d\vec{r}\\
&+ \delta_{m0}\frac{\mathrm{i}}{2c}\int v^{\mathrm{XC,s}}_g\vec{\nabla}\rho(\vec{r})\;(\vec{R}_{\mu\nu}\times\vec{r})_u\left[\vec{\nabla}\chi_\mu\chi_\nu + \chi_\mu\vec{\nabla}\chi_\nu\right]d\vec{r}\\
&+ \delta_{m0}\frac{\mathrm{i}}{2c}\int v^{\mathrm{XC,s}}_g\vec{\nabla}\rho(\vec{r})\;\chi_\mu\chi_\nu\left(\vec{B}\times\vec{R}_{\mu\nu}\right)^{B_u}d\vec{r}\\
&+ \delta_{m0}\frac{\mathrm{i}}{4c}\int\frac{\partial e^{\mathrm{XC}}}{\partial\tau_\uparrow(\vec{r})}\Big[(\vec{R}_{\mu\nu}\times\vec{r})_u\;\vec{\nabla}\chi_\mu\cdot\vec{\nabla}\chi_\nu\\
&+ \chi_\mu\left[(\vec{r}-\vec{R}_\mu)\times\vec{\nabla}\chi_\nu\right]_u - \chi_\nu\left[(\vec{r}-\vec{R}_\nu)\times\vec{\nabla}\chi_\mu\right]_u\Big]d\vec{r}\end{aligned} \tag{43}$$

with $v^{\mathrm{XC,s}}_g$

$$v^{\mathrm{XC,s}}_g = \frac{2\partial e^{\mathrm{XC}}}{\partial g_{\uparrow\uparrow}(\vec{r})} + \frac{\partial e^{\mathrm{XC}}}{\partial g_{\uparrow\downarrow}(\vec{r})}\,, \tag{44}$$

and $m = \{0,x,y,z\}$ denotes the spin cases arising from the total density (0) and the Pauli spin matrices (x,y,z). Further, u refers to the component of the magnetic field. $J_{\mu\nu,\kappa\lambda}$ and $K_{\mu\nu,\kappa\lambda}$ are the two-electron Coulomb and exchange integrals, respectively. e^{XC} specifies the energy of the given density functional approximation. Accordingly, $\partial e^{\mathrm{XC}}/\partial\rho(\vec{r})$ defines the derivative of the energy functional with respect to the local density, forming the local spin density approximation (LSDA) part, while the additions from the generalized gradient approximation (GGA) are identified as terms including $\partial e^{\mathrm{XC}}/\partial g(\vec{r})$ with $g(\vec{r}) = |\vec{\nabla}\rho(\vec{r})|^2$. The meta-GGA part, $\partial e^{\mathrm{XC}}/\partial\tau(\vec{r})$, depends on the kinetic-energy density τ. The latter necessitates generalizations for magnetic properties. Herein, we use the generalization of the kinetic-energy density as done by Maximoff and Scuseria,[109] i.e., τ is generalized by inclusion of the external magnetic field. See also Ref. 110. $\rho_\uparrow$ and $\rho_\downarrow$ finally denote the spin-up and spin-down density, respectively. The quantities $g_{\uparrow\uparrow}$ and $\tau_\uparrow$ are defined accordingly.

Using time-reversal symmetry, exploiting that the ground-state magnetization density vanishes at each point in space, the second contribution is accordingly obtained as

$$\begin{aligned}\left[\boldsymbol{P}^{2,m}_{\mu\nu}\right]_u = &\sum_{\kappa\lambda} O^{B_u,m}_{\kappa\lambda}\left[\delta_{m0}\; J_{\mu\nu,\kappa\lambda} - c_{\mathrm{X}}\frac{1}{2}K_{\mu\nu,\kappa\lambda}\right]\\
&+ \int\left(f^{\mathrm{XC,t}}_{\rho\rho}\rho^{B_u}_m(\vec{r}) + f^{\mathrm{XC,t}}_{\rho g}\vec{\nabla}\rho(\vec{r})\cdot\vec{\nabla}\rho^{B_u}_m(\vec{r}) + f^{\mathrm{XC,t}}_{\rho\tau}\tau^{B_u}_m(\vec{r})\right)\chi_\mu\chi_\nu\;d\vec{r}\\
&+ \int\left(f^{\mathrm{XC,t}}_{\rho g}\rho^{B_u}_m(\vec{r}) + f^{\mathrm{XC,t}}_{g g}\vec{\nabla}\rho(\vec{r})\cdot\vec{\nabla}\rho^{B_u}_m(\vec{r})\right)(\vec{\nabla}\chi_\mu\chi_\nu + \chi_\mu\vec{\nabla}\chi_\nu)\;d\vec{r}\\
&+ \int\left(v^{\mathrm{XC,t}}_g\vec{\nabla}\rho^{B_u}_m(\vec{r}) + f^{\mathrm{XC,t}}_{\tau g}\tau^{B_u}_m(\vec{r})\right)(\nabla\chi_\mu\chi_\nu + \chi_\mu\nabla\chi_\nu)\;d\vec{r}\\
&+ \int\left(f^{\mathrm{XC,t}}_{\rho\tau}\rho^{B_u}_m(\vec{r}) + f^{\mathrm{XC,t}}_{\tau g}\vec{\nabla}\rho(\vec{r})\cdot\vec{\nabla}\rho^{B_u}_m(\vec{r}) + f^{\mathrm{XC,t}}_{\tau\tau}\tau^{B_u}_m(\vec{r})\right)\vec{\nabla}\chi_\mu\cdot\vec{\nabla}\chi_\nu\;d\vec{r},\end{aligned} \tag{45}$$

where the respective contributions to the kernel are defined as

$$f^{\mathrm{XC,t}}_{\rho\rho} = \left(\frac{\partial^2 e^{\mathrm{XC}}}{\partial\rho_\uparrow(\vec{r})\partial\rho_\uparrow(\vec{r})} - \frac{\partial^2 e^{\mathrm{XC}}}{\partial\rho_\uparrow(\vec{r})\partial\rho_\downarrow(\vec{r})}\right), \tag{46}$$

$$f^{\mathrm{XC,t}}_{\rho g} = 2\left(\frac{\partial^2 e^{\mathrm{XC}}}{\partial\rho_\uparrow(\vec{r})\partial g_{\uparrow\uparrow}(\vec{r})} - \frac{\partial^2 e^{\mathrm{XC}}}{\partial\rho_\uparrow(\vec{r})\partial g_{\downarrow\downarrow}(\vec{r})}\right), \tag{47}$$

$$f^{\mathrm{XC,t}}_{\rho\tau} = \left(\frac{\partial^2 e^{\mathrm{XC}}}{\partial\rho_\uparrow(\vec{r})\partial\tau_\uparrow(\vec{r})} - \frac{\partial^2 e^{\mathrm{XC}}}{\partial\rho_\uparrow(\vec{r})\partial\tau_\downarrow(\vec{r})}\right), \tag{48}$$

$$f^{\mathrm{XC,t}}_{g g} = 4\left(\frac{\partial^2 e^{\mathrm{XC}}}{\partial g_{\uparrow\uparrow}(\vec{r})\partial g_{\uparrow\uparrow}(\vec{r})} - \frac{\partial^2 e^{\mathrm{XC}}}{\partial g_{\uparrow\uparrow}(\vec{r})\partial g_{\downarrow\downarrow}(\vec{r})}\right), \tag{49}$$

$$f^{\mathrm{XC,t}}_{\tau g} = 2\left(\frac{\partial^2 e^{\mathrm{XC}}}{\partial\tau_\uparrow(\vec{r})\partial g_{\uparrow\uparrow}(\vec{r})} - \frac{\partial^2 e^{\mathrm{XC}}}{\partial\tau_\uparrow(\vec{r})\partial g_{\downarrow\downarrow}(\vec{r})}\right), \tag{50}$$

$$f_{\tau\tau}^{\mathrm{XC,t}} = \left(\frac{\partial^2 e^{\mathrm{XC}}}{\partial\tau_\uparrow(\vec{r})\partial\tau_\uparrow(\vec{r})} - \frac{\partial^2 e^{\mathrm{XC}}}{\partial\tau_\uparrow(\vec{r})\partial\tau_\downarrow(\vec{r})} \right), \tag{51}$$

$$v_g^{\mathrm{XC,t}} = \left(2\frac{\partial^2 e^{\mathrm{XC}}}{\partial g_{\uparrow\uparrow}(\vec{r})} - \frac{\partial^2 e^{\mathrm{XC}}}{\partial g_{\uparrow\downarrow}(\vec{r})} \right). \tag{52}$$

$O_{\kappa\lambda}^{B,m}$ in Eq. (45) denotes the occupied-occupied part of the orbital rotations for the perturbed density matrix. This is obtained from the derivative of the overlap matrix, i.e., it arises solely from the GIAOs. In the 2c spinor space, this part is obtained as

$$O_{ij}^{B_u} = -\frac{1}{2} S_{ij}^{B_u}. \tag{53}$$

Here, we stress that this choice for $O_{ij}^{B_u}$ corresponds to the symmetric connection and minimizes the difference between the field-dependent occupied and virtual spinors.[28] Transformation of $O_{ij}^{B_u}$ to the atomic orbital (AO) space yields the respective part of the perturbed density matrix and also forms the occupied-occupied block of $\{\mathbf{U}^{B_u}, \mathbf{V}^{B_u}\}$. Note that the two-electron Coulomb contribution in Eq. (45) vanishes for time-reversal symmetric Ref. 22 The corresponding magnetic field perturbed density variables ρ^B, $\nabla\rho^B$, and τ^B,

$$\rho_m^{B_u} = \rho_{R,m}^{B_u} + \rho_{D,m}^{B_u} \tag{54}$$

$$\nabla\rho_m^{B_u} = \nabla\rho_{R,m}^{B_u} + \nabla\rho_{D,m}^{B_u} \tag{55}$$

$$\tau_m^{B_u} = \tau_{R,m}^{B_u} + \tau_{D,m}^{B_u} \tag{56}$$

are assembled from contributions from the reorthonormalization part, utilizing $O_{\mu\nu}^{B_u}$, as

$$\rho_{R,m}^{B_u}(\vec{r}) = \sum_{\mu\nu} O_{\mu\nu}^{B_u,m}\, \chi_\mu\chi_\nu, \tag{57}$$

$$\vec{\nabla}\rho_{R,m}^{B_u}(\vec{r}) = \frac{1}{2}\sum_{\mu\nu} O_{\mu\nu}^{B_u,m}\left[\vec{\nabla}\chi_\mu\chi_\nu + \chi_\mu\vec{\nabla}\chi_\nu\right], \tag{58}$$

$$\tau_{R,m}^{B_u}(\vec{r}) = \sum_{\mu\nu} O_{\mu\nu}^{B_u,m}\, \vec{\nabla}\chi_\mu\vec{\nabla}\chi_\nu. \tag{59}$$

The contributions from the direct GIAO terms read

$$\rho_{D,m}^{B_u}(\vec{r}) = \sum_{\mu\nu} D_{\mu\nu}^m \left[\frac{1}{2c}(\vec{R}_{\mu\nu}\times\vec{r})_u\, \chi_\mu\chi_\nu\right], \tag{60}$$

$$\vec{\nabla}\rho_{D,m}^{B_u}(\vec{r}) = \frac{1}{2}\sum_{\mu\nu} D_{\mu\nu}^m \left[\frac{1}{2c}(\vec{R}_{\mu\nu}\times\vec{r})_u\left(\vec{\nabla}\chi_\mu\chi_\nu + \chi_\mu\vec{\nabla}\chi_\nu\right)\right], \tag{61}$$

$$\begin{aligned}\tau_{D,m}^{B_u}(\vec{r}) = &\sum_{\mu\nu} D_{\mu\nu}^m \left[\frac{1}{2c}(\vec{R}_{\mu\nu}\times\vec{r})_u\vec{\nabla}\chi_\mu\cdot\vec{\nabla}\chi_\nu\right] \\ &+ \sum_{\mu\nu} D_{\mu\nu}^m \left[\frac{1}{2c}\chi_\mu\{(\vec{r}-\vec{R}_\mu)\times\vec{\nabla}\chi_\nu\}_u\right] \\ &- \sum_{\mu\nu} D_{\mu\nu}^m \left[\frac{1}{2c}\chi_\nu\{(\vec{r}-\vec{R}_\nu)\times\vec{\nabla}\chi_\mu\}_u\right].\end{aligned} \tag{62}$$

Again, the generalization of the kinetic-energy density has been performed as described by Maximoff and Scuseria to achieve a gauge-invariant formulation also for meta-GGA functionals. For the reorthonormalization all density blocks (i.e., $m = 0, x, y, z$) will contribute, while only the spin density blocks (i.e., $m = x, y, z$) will give rise to non-zero terms for the direct GIAO part due to symmetry reasons.

Compared to the scalar 1c approach, the SO spin-density functional theory (SDFT) ansatz always necessitates an iterative solution of the CPKS equations, even for pure density functional approximations with the Maximoff–Scuseria generalization of τ.

While the Maximoff–Scuseria generalization of τ restores gauge-origin invariance, it may lead to artifacts[111] and the current-dependent generalization[112–114] is preferred in TURBOMOLE.[68,115–118] The impact of these artifacts and the improvement with the current-dependent generalization depend on the enhancement factor of the functional construction, see Refs. 68, 118, and 119 for discussions. Based on our previous studies,[68,116–118,120] the Maximoff–Scuseria generalization is sufficient for functionals such as TPSS[121] or the Tao-Mo[122] functional and their hybrids. However, it can lead to large errors for the Minnesota functionals[123,124] and TASK.[125] The SCAN functional family[126–128] represents an intermediate case in this regard. For global and range-separated hybrid functionals, the impact is generally smaller as HF exchange and its response use the same density matrix blocks as the current density and its response, i.e., HF exchange always includes the current density. Moreover, calculations of open-shell systems and EPR or paramagnetic NMR properties are typically more sensitive to the generalization of τ. An extension of the presented approach to our current density functional framework of Ref. 68 is in progress but requires major extensions for the XC potential derivative,[111,116,118] while the XC kernel for the left-hand side was already derived and used within a common gauge origin ansatz.[68]

Following the nomenclature of Ref. 29, neglecting the complete XC kernel as done in Ref. 39 is denoted spin–orbit density functional theory ("SO DFT") and including the contribution is denoted spin–orbit non-collinear or spin-density functional theory ("SO SDFT"). Just like the non-relativistic approach, the CPKS equations for semilocal or pure functionals in SO DFT can be solved non-iteratively in one shot. Note that the direct contribution from the GIAO terms, i.e., Eqs. (60)–(62) are not explicitly discussed in the 2c ZORA work of Ref. 41 and the respective implementation "may give some (small) gauge dependent results."[129] Herein, we denote the approach neglecting the XC kernel contribution from the direct GIAO terms "SO SDFT-nogxc."

III. IMPLEMENTATION

The relativistic two-component approach outline herein was implemented into TURBOMOLE[130–133] and its mpshift module.[34,68,84,91,95,110,118,120,134] All new one-electron integrals for the X2C Hamiltonian using the restricted magnetic balance condition and GIAOs are evaluated with a combination of Gauss–Rys and Gauss–Legendre integration, cf. Ref. 102. The DLU scheme[81,96,104] and the SNSO/mSNSO approximation,[80,92,93] applied to the integrals directly,[80,135] are available throughout. We refer to Ref. 34 for details

on the application of the DLU scheme to analytical derivatives. Further, a Gaussian charge distribution[67] is available within the finite nucleus model for both the scalar and the vector potential. This model is used throughout this work. A value of 137.035 999 084 0 is used for the speed of light in atomic units.[136] All X2C/DLU-X2C steps are carried out in the primitive or decontracted basis set and the contraction is performed after the decoupling steps or solving the X2C response equations.

Two-electron integrals can be evaluated exactly, i.e., without approximations except for integral screening, or with the (multipole-accelerated) resolution of the identity approximation for the Coulomb term[56,57,110,137–139] (MARI-J/RI-J) and the seminumerical (snK) exchange approximation.[63] The latter is restricted to the response terms in the CPHF/CPKS equations, i.e., the GIAO-derivatives for the right-hand side of the CPHF/CPKS equations are not yet available. This setting allows for the use of small grids without loss of accuracy as shown below.

Density functional approximations are supported up to the class of range-separated hybrids. Interfaces to XCFun[140] and Libxc[141–143] are provided for broad support of density functional approximations.

The conductor-like screening model (COSMO) is available to simulate the environment or the effects of solution[144,145] by interfacing the existing implementations of Refs. 34, 84, and 110. Here, the relativistic picture-change correction for the embedding potential and the cavity construction is neglected.

Shared-memory parallelization is supported with the OpenMP paradigm[146,147] and the CPHF/CPKS equations are solved based on the algorithm outlined in Ref. 108 in the static response version, see also Ref. 102.

NMR shielding constants can also be calculated at mass-less and charge-less points in space to compute the nucleus-independent chemical shift (NICS).[148] This can be used to estimate the degree of electron delocalization and aromaticity based on the magnetic criterion.[149–154] Here, we use a mass of 10^{-6} a.u. to compute the exponent for the finite nucleus model based on Ref. 67.

Gauge-origin and translation invariance were validated for HI, HAt, H_2Te, and H_2Po with double-ζ basis sets for LSDA, GGA, meta-GGA, and their hybrid functional classes at the DFT and SDFT levels of theory as well as for generalized Hartree–Fock theory.

IV. COMPUTATIONAL METHODS

First, we assess the accuracy of the spin–orbit X2C Hamiltonian compared to the four-component Dirac–Coulomb approach of Ref. 29. Thus, the HX molecules (X = F, Cl, Br, I, At) are considered with the same structures as in that reference. The bond lengths are 0.9168 Å (HF),[155] 1.2746 Å (HCl),[155] 1.4144 Å (HBr),[155] 1.6092 Å (HI),[155] and 1.7279 Å (HAt).[156] Fully decontracted aug-cc-pVQZ basis sets[157,158] are employed for H, F, Cl, whereas the dyall-acvqz bases[159,160] are employed for Br, I, At. The S-VWN (V-fit),[161–163] BP86,[164,165] and B3LYP[166–168] functionals are employed to represent the different rungs of Jacob's ladder[169] with very large grids for the numerical integration (grid size 5a[170–172]). Details on the construction of these grids are fully published in Refs. 170–172. The number of radial grid points n_{rad} is calculated according to

$$n_{rad} = 20 + 5(s-1) + Z \tag{63}$$

with the nuclear charge Z and $s = 1, 2, 3, 6, 8, 10, 14$ for the grids 1a, 2a, 3a, 4a, 5a, 6a, and 7a.[172] Note that the last term, $+Z$, is only used for non-hydrogen atoms. For the spherical integration, the number of grid points for non-hydrogens is 110, 194, 302, 434, 590, 974, 1202 for grids 1a–7a, while it is 50, 110, 194, 302, 434, 974, 1202 for hydrogen.[171] The number of spherical grid points near the nuclei is reduced by default ("pruning") and grid ordering is applied.[171] The V-fit and the III-fit for VWN in B3LYP are used for the comparison to 4c results. In the main text, only results with the V-fit are shown for comparison with 4c results, cf. the DIRAC[173] manual on B3LYP.[174] All other B3LYP applications in this work make use of the V-fit. Additionally, the KT2 functional[175] is applied with the decontracted aug-cc-pVQZ/dyall-avqz and the decontracted aug-cc-pVTZ/dyall-acvtz basis sets[157–160] using the XCFun library.[140] Converged results are ensured by tight thresholds of 10^{-9} E_h for the SCF energy and 10^{-8} for the root-mean square (rms) of the SCF density matrix change, as well as a criterion of 10^{-9} for the norm of the residuum in the CPKS equations.[108] Exact two-electron Coulomb and exchange integrals (for hybrid functionals) are used throughout. The X2C Hamiltonian is combined with the mSNSO approximation.[80,92,93]

Second, the error introduced by the DLU, RI-J, and snK approximations is assessed for a subset of the set of tin compounds compiled in Ref. 176. We have previously used the same set to study the respective errors for NMR couplings.[85] The molecular structures are taken from Ref. 84 and are optimized at the DLU-X2C level. Again, the mSNSO approximation is applied to account for the missing two-electron picture-change correction. Herein, we apply the PBE0[177,178] functional with large grids (grid size 5a[170–172]) and the x2c-TZVPPall-2c basis sets.[179] Thresholds of 10^{-9} E_h for the energy and 10^{-8} for the rms of the density matrix change indicate convergence of the SCF procedure. CPKS equations are converged up to 10^{-7} for the norm of the residuum. To simulate the counter ions, COSMO is applied with the default settings for charged systems,[144,145,180] i.e., with a relative permitivity approaching infinity. Note that this ensures negative energy eigenvalues for occupied states.

Third, the efficiency is assessed for the pincer-type 2,6-diaminopyridine-bridged bis-stannylene ligand **SnNSn** of Ref. 181. To do so, the PBE0[177,178] functional is applied with large grids (grid size 3a[170–172]) and the x2c-TZVPPall-2c basis set.[179] SCF convergence thresholds of 10^{-7} E_h and 10^{-6} for the rms of the density matrix change are chosen, while a criterion of 10^{-7} is applied for the norm of the CPKS residuum. The molecular structure is taken from Ref. 181. Two-component calculations use the mSNSO approach to account for the missing two-electron picture-change correction. Herein, we study the efficiency of the DLU, MARI-J, and snK approximations. The default settings are applied for the MARI-J approximation.[137,180] For simplicity, COSMO is not applied in the assessment of efficiency.

Fourth, the ^{31}P NMR shifts of the low-valent group-14 complexes $[(\{SIDipp\}P)_2M]$ (M = Sn, Pb and SIDipp = 1,3-bis(2,6-di-isopropylphenyl)-imidazolidin-2-ylidene) as well as $[(\{SIDipp\}P)SnCl]_2$ and $[(\{SIDipp\}P)PbBr]_2$ of Ref. 182 are computed with the mSNSO-DLU-X2C Hamiltonian. These four complexes are denoted **4**, **5**, **6**, and **7** in this reference. The BP86,[164,165] Perdew–Burke–Ernzerhof (PBE),[177] TPSS,[121] B3LYP,[164,167,168] PBE0,[177,178] TPSSh,[121,183] and CAM-B3LYP[184]

functionals are applied together with the x2c-TZVPall-2c orbital[179] and RI-J auxiliary basis sets.[179] We use the snK approximation for the response density part of the CPKS framework (grid size medium).[63] Structures were optimized for each functional and are taken from previous work when possible.[85,182] Thus, only the structures of [({SIDipp}P)$_2$Pb], [({SIDipp}P)SnCl]$_2$, and [({SIDipp}P)PbBr]$_2$ for CAM-B3LYP with the D4 dispersion correction[185] had to be optimized in the present work. These structures are given in the supplementary material. Further computational settings are chosen accordingly,[85] i.e., large grids for the XC part (grid size 4a[170–172]) and tight SCF convergence thresholds of 10^{-9} E_h and 10^{-8} for the rms density change. The 2c CPKS equations are converged up to 10^{-7} for the norm of the residuum. COSMO is used to simulate the solution effects for benzene (permittivity of $\varepsilon = 2.300$, refractive index of $n = 1.4957$).

Fifth, we study the impact of spin–orbit coupling on the ring currents of all-metal aromatic systems[186–194] as collected in Ref. 194. That is, our previous studies are complemented with 2c NICS calculations (grid size 3a[170–172]) based on the mSNSO-DLU-X2C Hamiltonian. The PBE0 functional[177,178] is used together with the snK approximation for the CPKS part in the present work. Thus, new scalar-relativistic calculations were also carried out herein. The scalar calculations utilize the x2c-TZVPall-s orbital and auxiliary basis sets,[172] while the x2c-TZVPall-2c orbital[179] and RI-J auxiliary basis sets[179] are applied for the two-component calculations. Structures are taken from Ref. 194 and we use the same point in space for the ghost atom, at which the NICS(0) is computed. The corresponding SCF energies were converged up to 10^{-8} E_h and a threshold of 10^{-7} was used for the norm of the residuum in the CPKS procedure. COSMO is applied with the default settings.[144,145,180] Additionally, we study Bi_6^{2-} as well as the related complexes **1**$^-$ ([{CpRu}$_3$Bi$_6$]$^-$, Cp = cyclopentadienide) and **2**$^-$ ([{(cod)Ir}$_3$Bi$_6$]$^-$, cod = 1,5-cyclooctadiene) of Ref. 195 at the TPSS/x2c-TZVPall-s/COSMO level.

V. RESULTS AND DISCUSSION

A. Comparison to the Dirac–Kohn–Sham approach

Results with the non-relativistic (NR), scalar-relativistic (SR), spin–orbit (SO), and fully relativistic Dirac–Coulomb Hamiltonians are listed in Table I. Compared to the impact of spin–orbit interaction, scalar-relativistic effects are of minor importance. Especially for the hydrogen nuclei, scalar-relativistic calculations do not lead to changes of more than 0.1 ppm compared to the non-relativistic limit. The impact of spin–orbit coupling on the hydrogen atoms for these systems, i.e., the spin–orbit heavy atom on the light atom (HALA) effect, is well known and discussed comprehensively in Ref. 43. Also, for the heavy elements SR effects are comparably small.

Generally, the 2c approaches lead to an excellent agreement with the four-component DKS methodology. Errors typically amount to less than 1% for all functionals in the SDFT formalism. Similar findings hold for the DFT formalism neglecting the XC kernel contribution. As expected, the largest error is found for HAt with less than 5% for At and about 1%–2% for H with all functionals. The errors tend to decrease for the B3LYP functional, indicating that at least a part of the total error can be attributed to different schemes for the numerical integration of the XC potential and kernel.

Up to HBr, neglecting the kernel contribution as done in SO DFT and DKS DFT does not lead to large errors for both the heavy and the light atom. Starting with HI, the deviation between DFT and SDFT becomes significant for the hydrogen atom, i.e., an error of almost 3 ppm is observed. For HAt, the deviation amount to 10 ppm for S-VWN, BP86, and B3LYP. An even larger impact of the XC kernel is found for KT2 with almost 15 ppm. This is an error of more than 20% for the total shielding constant and the DFT ansatz only captures about 56% of the spin–orbit effects on the hydrogen shielding. This is in line with the discussion of the Wolff *et al.* in Ref. 39. These authors suggested that this approximation works well for heavy nuclei and, just like the full SDFT approach, this ansatz is gauge-origin invariant. However, results for molecules with pronounced SO-HALA effects substantially benefit from including the SDFT exchange-correlation kernel, see also Ref. 196.

As long as the molecules are placed close to the origin of the coordinate system, the SDFT-nogxc approximation yields reasonable results. However, the shielding constants change notably when moving (non-linear) molecules by about 30–50 bohrs. To support this point, we consider the shieldings of H_2Te at the S-VWN, BP86, KT2, TPSS, B3LYP, and CAM-B3LYP levels using decontracted cc-pVDZ bases for H[157] and uncontracted dyall-vdz bases for Te.[159,160] The H–Te bond lengths are 1.659 Å and the H–Te–H angle is 90.26°. We use very large grids (grid size 7a,[170–172] reference settings[180]) and very tight SCF convergence thresholds of 10^{-12} E_h for the energy and 10^{-10} for the rms of the density matrix change. The H_2Te molecule is first placed so that the center of mass is at the origin of the coordinate system and then moved by 50 bohrs along each Cartesian axes with simultaneous rotation by 30° around the axes. Results are shown in Table II. The DFT and SDFT methods lead to the same results for both placements. The changes in the shieldings are in the order of 10^{-4} ppm for Te with BP86 and consequently negligible, whereas the SDFT-nogxc approximation leads to pronounced changes and the two hydrogen atoms are no longer equivalent as the shieldings differ by about 1.5 ppm (S-VWN), 1.4 ppm (BP86), 2.1 ppm (KT2), 1.0 ppm (TPSS), 1.0 ppm (B3LYP), and 0.9 ppm (CAM-B3LYP). As expected, the admixture of HF exchange tends to reduce the changes in the shielding constants, as the latter remains gauge-invariant. Overall, this shows that the direct response of the GIAOs for the calculation of the density on a grid is crucial for the XC kernel on the right-hand side of the CPKS equations.

The spin–orbit X2C Hamiltonian is an accurate approximation of the parent four-component Dirac–Coulomb ansatz. Furthermore, it was found to be crucial that the full XC kernel is included for molecules with a large SO-HALA effect.

B. Assessment of accuracy for tin compounds

The impact of spin–orbit coupling and the full consideration of the XC kernel are studied for a set of small tin compounds, as Sn is among the most important metal atoms for NMR spectroscopy. Here, we also assess the accuracy of the DLU scheme, the RI-J approximation, as well as the snK approach for the CPKS equations. For convenience, the PBE0 func-

TABLE I. Isotropic NMR shielding constants (ppm) with various density functional approximations at the non-relativistic (NR), scalar-relativistic (SR) X2C, as well as the spin–orbit (SO) mSNSO-X2C, and 4c Dirac–Kohn–Sham (DKS) levels. Non-relativistic, SR, and SO calculations employ the finite nucleus model with a Gaussian charge distribution for both the scalar and the vector potential. DFT denotes neglecting the XC kernel, SDFT-nogxc including the kernel without the direct GIAO response terms associated with the spin-current density, and SDFT the complete kernel. Note that the SDFT-nogxc approximation is consequently gauge-variant, see also Refs. 41 and 129. The relative error (Rel. Error) in percent is given for SO SDFT compared to 4c DKS SDFT. The decontracted aug-cc-pVQZ/dyall-acvqz bases are used with S-VWN, BP86, and B3LYP, while the aug-cc-pVTZ/dyall-acvtz bases are additionally applied for the KT2 calculations. Usage of the aug-cc-pVTZ/dyall-acvtz bases with KT2 is denoted KT2 TZ. The VWN V-fit is used for S-VWN and B3LYP. See supplementary material for results with B3LYP using the VWN III-fit. DKS results are taken from Ref. 29. Structures are the same.

Functional	Molecule	Nucleus	NR	SR	SO DFT	DKS DFT	SO SDFT-nogxc	SO SDFT	DKS SDFT	Rel. error
S-VWN	HF	H	29.21	29.23	29.31	29.08	29.39	29.33	29.10	0.78
		F	415.84	415.89	420.10	418.82	421.73	420.33	419.00	0.32
S-VWN	HCl	H	30.82	30.84	31.37	31.09	31.54	31.53	31.25	0.91
		Cl	954.82	955.73	985.52	981.57	986.54	986.56	982.39	0.42
S-VWN	HBr	H	30.92	30.93	33.94	33.75	35.07	34.94	34.73	0.61
		Br	2604.88	2614.54	2 908.33	2 901.51	2 917.44	2 917.18	2 908.83	0.29
S-VWN	HI	H	31.06	31.01	39.35	39.19	42.41	42.43	42.20	0.55
		I	4490.97	4518.93	5 705.18	5 705.32	5 740.73	5 743.07	5 738.77	0.07
S-VWN	HAt	H	30.55	30.43	50.20	50.07	57.74	57.95	57.22	1.27
		At	8565.04	8515.74	16 840.40	16 290.46	17 208.57	17 214.14	16 613.22	3.62
BP86	HF	H	29.88	29.89	29.98	29.77	30.11	30.03	29.81	0.73
		F	411.53	411.55	415.82	414.52	417.88	416.16	414.77	0.33
BP86	HCl	H	31.48	31.50	32.06	31.79	32.34	32.33	32.03	0.92
		Cl	943.90	944.66	974.65	970.78	976.04	976.07	972.00	0.42
BP86	HBr	H	31.69	31.71	34.93	34.73	36.73	36.52	36.15	1.01
		Br	2574.31	2581.69	2 876.88	2 870.34	2 890.86	2 890.43	2 881.92	0.30
BP86	HI	H	31.89	31.85	40.78	40.61	45.35	45.42	44.72	1.56
		I	4430.00	4446.72	5 639.19	5 639.34	5 696.11	5 698.00	5 691.67	0.11
BP86	HAt	H	31.41	31.33	52.66	52.49	62.81	63.34	61.66	2.73
		At	8434.35	8298.24	16 699.80	16 133.59	17 249.89	17 244.31	16 596.95	3.90
B3LYP	HF	H	29.44	29.46	29.55	29.34	29.66	29.59	29.37	0.76
		F	411.86	411.88	416.21	414.96	417.49	416.26	415.14	0.27
B3LYP	HCl	H	31.35	31.37	32.00	31.72	32.25	32.24	31.95	0.90
		Cl	940.34	941.03	971.40	967.25	972.44	972.45	968.18	0.44
B3LYP	HBr	H	31.62	31.64	35.22	35.02	36.80	36.66	36.42	0.66
		Br	2570.74	2577.75	2 877.33	2 869.87	2 887.38	2 887.18	2 878.58	0.30
B3LYP	HI	H	31.93	31.87	41.96	41.79	46.29	46.32	46.04	0.62
		I	4418.93	4433.44	5 650.36	5 648.45	5 690.98	5 692.95	5 688.14	0.08
B3LYP	HAt	H	31.47	31.36	55.95	55.79	66.51	66.80	66.24	0.84
		At	8420.17	8250.84	16 989.77	16 401.59	17 392.09	17 396.52	16 765.53	3.76
KT2	HF	H	29.93	29.94	30.03	29.82	30.14	30.07	29.87	0.67
		F	412.25	412.27	416.59	415.34	419.01	417.05	415.69	0.33
KT2	HCl	H	31.39	31.41	31.96	31.68	32.28	32.26	31.98	0.88
		Cl	957.95	958.89	988.86	984.76	990.39	990.32	986.22	0.42
KT2	HBr	H	31.66	31.67	34.82	34.63	36.88	36.66	36.44	0.60
		Br	2608.97	2618.41	2 913.32	2 904.77	2 925.15	2 925.74	2 916.72	0.31
KT2	HI	H	31.83	31.77	40.57	40.42	46.21	46.24	45.96	0.61
		I	4495.91	4522.70	5 713.89	5 707.05	5 764.14	5 767.38	5 760.82	0.11
KT2	HAt	H	31.31	31.21	52.75	52.61	67.10	67.48	66.80	1.01
		At	8545.26	8454.94	16 943.96	16 282.02	17 485.15	17 489.64	16 818.86	3.99
KT2 TZ	HF	H	30.13	30.14	30.23	29.95	30.29	30.27	30.00	0.90
		F	413.10	413.13	417.33	415.71	418.26	417.72	416.05	0.40
KT2 TZ	HCl	H	31.51	30.14	32.06	31.73	32.34	32.34	32.01	1.03

TABLE I. (*Continued*.)

Functional	Molecule	Nucleus	NR	SR	SO DFT	DKS DFT	SO SDFT-nogxc	SO SDFT	DKS SDFT	Rel. error
		Cl	960.08	961.11	990.91	986.68	992.34	992.37	988.12	0.43
KT2 TZ	HBr	H	31.71	31.72	34.75	34.50	36.51	36.51	36.22	0.80
		Br	2609.09	2618.71	2 913.75	2 901.80	2 925.48	2 926.10	2 913.54	0.43
KT2 TZ	HI	H	31.87	31.81	40.28	40.05	45.56	45.71	45.33	0.83
		I	4497.20	4524.02	5 715.26	5 702.63	5 766.20	5 768.55	5 755.50	0.23
KT2 TZ	HAt	H	31.35	31.26	51.98	51.78	65.53	66.10	65.29	1.25
		At	8546.88	8455.56	16 946.75	16 261.13	17 482.71	17 489.18	16 792.82	4.15

TABLE II. Isotropic NMR shielding constants (ppm) at the spin–orbit X2C S-VWN, BP86, KT2, TPSS, B3LYP, and CAM-B3LYP (CAM) levels of theory using decontracted cc-pVDZ/dyall-vdz basis sets for H_2Te. The H–Te bond lengths are 1.659 Å and the H–Te–H angle is 90.26°. "Origin" refers to the placement of the molecule so that the center of mass is at the origin. "Moved" indicates that the molecule was moved by 50 bohrs along each Cartesian axis with simultaneous rotation by 30° around each axis.

	Origin			Moved		
S-VWN	DFT	SDFT-nogxc	SDFT	DFT	SDFT-nogxc	SDFT
H	34.11	35.98	36.06	34.11	36.36	36.06
H	34.11	35.98	36.06	34.11	34.83	36.06
Te	4600.14	4637.38	4640.44	4600.15	4632.26	4640.45
BP86	DFT	SDFT-nogxc	SDFT	DFT	SDFT-nogxc	SDFT
H	34.94	37.47	37.67	34.94	37.72	37.67
H	34.94	37.47	37.67	34.94	36.36	37.67
Te	4513.58	4569.52	4573.74	4513.58	4562.63	4573.74
KT2	DFT	SDFT-nogxc	SDFT	DFT	SDFT-nogxc	SDFT
H	34.88	38.16	38.32	34.88	38.64	38.32
H	34.88	38.16	38.32	34.88	36.54	38.32
Te	4634.53	4683.79	4687.50	4634.53	4678.15	4687.50
TPSS	DFT	SDFT-nogxc	SDFT	DFT	SDFT-nogxc	SDFT
H	34.63	37.77	37.86	34.63	37.78	37.86
H	34.63	37.77	37.86	34.63	36.71	37.86
Te	4565.71	4631.40	4634.99	4565.71	4626.07	4634.99
B3LYP	DFT	SDFT-nogxc	SDFT	DFT	SDFT-nogxc	SDFT
H	35.73	38.14	38.22	35.73	38.29	38.22
H	35.73	38.14	38.22	35.73	37.31	38.22
Te	4517.35	4552.78	4554.97	4517.35	4550.86	4554.97
CAM	DFT	SDFT-nogxc	SDFT	DFT	SDFT-nogxc	SDFT
H	35.72	38.18	38.22	35.72	38.27	38.22
H	35.72	38.18	38.22	35.72	37.39	38.22
Te	4577.40	4609.71	4610.79	4577.40	4608.87	4610.79

tional and triple-ζ basis sets area applied. Results are shown in Table III.

We stress that the main purpose of this sections is to study the accuracy of the DLU, RI-J, and snK approximations as compared to the impact of spin–orbit coupling and the XC kernel (SDFT vs DFT). Accordingly, the agreement with the experimental findings can likely be improved with a larger basis set, a higher theoretical level for environmental effects, or other functionals than PBE0. For instance, local hybrid functionals[207] such as LHJ-HFcal,[208] TMHF,[208] or the range-separated hybrid CAM-B3LYP[184]

TABLE III. Assessment of approximations for the isotropic Sn NMR shielding constant of $SnMe_4$ and the Sn NMR chemical shifts (all in ppm) of a set of tin compounds compiled in Ref. 176. Experimental findings[197–206] (Expt.) were collected in Ref. 176. The SO SDFT level of theory is used to assess the accuracy of the approximations. It is understood that more and more approximations are turned on, i.e., the RI-J column implies that DLU is applied. The DLU and RI-J approximations are applied for both the SCF and NMR calculations, whereas the snK ansatz (grid size medium) is only used for the response density contributions of the CPKS approach. Me denotes methyl (CH_3) groups.

	Level of theory				Approximations to SO SDFT			
Molecule	NR	SR	SO DFT	SO SDFT	DLU	RI-J	snK	Expt.
$SnMe_4$	2697.4	2542.3	2392.9	2412.6	2412.7	2414.0	2413.1	⋯
$(Me_3Sn)_2$	−115.8	−90.0	−110.4	−110.5	−110.4	−110.2	−111.4	−113
SnH_4	−521.5	−565.2	−571.2	−560.1	−560.0	−559.3	−560.4	−500
SnH_3^+	815.6	918.9	915.6	833.5	833.4	832.5	831.8	−186
SnH_3^-	−885.3	−951.3	−926.4	−921.1	−920.9	−919.5	−920.2	⋯
Me_3SnCl	151.0	176.8	163.3	149.8	149.8	149.8	148.9	164
Me_2SnCl_2	160.7	194.5	160.0	136.1	136.2	136.3	135.7	141.2
$MeSnCl_3$	75.4	107.3	27.3	−2.3	−2.3	−1.9	−2.7	21
$SnCl_4$	−37.7	−4.3	−193.6	−231.4	−231.5	−230.8	−231.7	−150
Me_3SnBr	156.7	194.5	123.4	108.6	108.6	108.5	107.5	128
Me_2SnBr_2	208.8	271.1	64.0	32.2	32.2	32.2	31.6	70
$MeSnBr_3$	181.8	258.2	−226.7	−278.1	−278.2	−277.6	−278.4	−165
$SnBr_4$	113.3	196.0	−844.8	−932.1	−932.4	−930.7	−931.7	−638
Me_3SnI	138.0	189.8	16.0	−1.4	−1.3	−1.5	−2.4	39
Me_2SnI_2	221.5	322.0	−207.7	−249.4	−249.3	−249.4	−250.3	−159
$MeSnI_3$	254.3	395.9	−848.2	−915.7	−915.8	−914.9	−915.7	−700
SnI_4	242.0	408.2	−2137.1	−2215.2	−2215.1	−2212.4	−2212.5	−1701
SnI_3Cl	188.3	310.6	−1676.7	−1769.6	−1769.8	−1767.7	−1768.6	−1130, −1347
$SnCl_3I$	44.2	101.2	−684.2	−757.9	−758.0	−757.1	−758.0	−543, −557

perform best for the NMR coupling constants of this test set.[85] In this regard, the bad performance of standard (gas-phase) DFT methods for SnH_3^+ was already noted and discussed in Ref. 176. It was shown that environmental effects are of great importance for the molecular structure and an explicit treatment of counter ions vastly improved the results.[176]

As shown by the difference between the scalar and the SO SDFT results, spin–orbit coupling plays a major role for most molecules. Especially molecules containing iodine atoms necessitate a treatment of spin–orbit effects. Neglecting the XC kernel contribution leads to large errors for $SnBr_4$, $MeSnI_3$, SnI_4, SnI_3Cl, and $SnCl_3I$. Here, errors can amount to almost 100 ppm. One the one hand, this is still comparably small given that SO effects change the shift by 500–2000 ppm. One the other hand, including the kernel does not notably increase the computational demands for PBE0, as HF exchange requires to iteratively solve the CPKS equations. For instance, the wall time for the NMR shieldings and shifts increases to 14 min compared to 11 min for SnI_4 [8 OpenMP threads of an Intel Xeon Gold 6212U central processing unit (CPU) at 2.40 GHz]. Therefore, we recommend to include the XC kernel in all calculations including calculations with pure density functionals such as PBE or TPSS. For pure functionals, full SDFT may lead to a more substantial increase of the wall time, as an iterative solution of the CPKS equations is required even in the absence of HF exchange.

Next, we discuss the errors introduced by various approximations. Note that the errors of the respective energy calculations prior to the NMR shielding calculations are not discussed herein. We refer to Refs. 96 and 104 for the DLU errors of energies and to Refs. 179 and 209 for the respective RI-J errors. For NMR shifts, the errors introduced by the three approximations were previously assess in a one-component formalism and found to be negligible.[34,110,116]

According to the results in Table III, the DLU error for NMR shifts in the two-component formalism is completely negligible, as it changes the NMR shifts by at most 0.3 ppm. The mean absolute error and the respective standard deviation are 0.09 and 0.08 ppm. As evident by the error of 0.1 ppm for the isotropic shift of $SnMe_4$, this is not due to error cancellation from the computation of the chemical shifts according to $\delta = \sigma_{ref} - \sigma_{sample}$. This confirms our previous studies on closed-shell and paramagnetic NMR as well as EPR properties.[34,84,85,91,95,120,210] Thus, the DLU scheme can be safely used for all NMR and EPR properties.

To compare with, the errors introduced by the RI-J approximation are somewhat larger, i.e., these typically amount to about 0.5–1 ppm. The largest error is found for SnI_4 with 2.7 ppm. The NMR shift of this molecules is about −915 ppm and spin–orbit effects amount to about 500 ppm. The mean absolute error is 0.8 ppm with a standard deviation of 0.8 ppm. The error of the shifts is very similar to the error of the isotropic shielding constant for $SnMe_4$, indicating no error cancellation when calculating the chemical shifts. Thus, this error is also negligible, at least with tailored auxiliary basis sets as provided in Refs. 179 and 209.

Finally, the snK error on top of an RI-J calculation is slightly smaller than that of the RI-J approximation. Note that we only use the snK approximation for the response density of the CPKS procedure as suggested in Refs. 63 and 116. This allows for the use

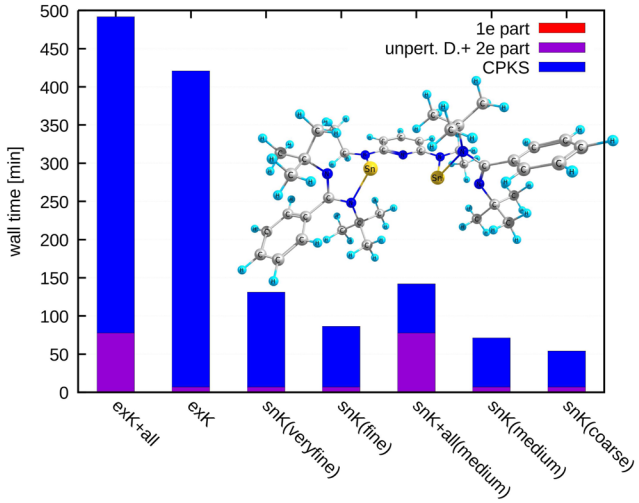

FIG. 1. Wall times in minutes for the calculation NMR shieldings of the tin pincer complex **SnNSn** introduced in Ref. 181. Calculations are performed at the 2c DLU-X2C PBE0/x2c-TZVPPall-2c level of theory. "+all" denotes that shieldings were calculate for all atoms, else only Sn were considered. snK denotes seminumerical exchange, and exK denotes analytical exchange. Calculations were carried out with a central processing unit (CPU) of type AMD EPYC 7453 utilizing a total of 48 OpenMP threads. The code was compiled with the ifx (IFORT) compiler, version 2022.1.0.

of a small integration grid (grid size medium[63]) for the snK part. SCF energies and densities generally necessitate larger grids.[62,63] The largest error is observed for $(Me_3Sn)_2$ with 1.1 ppm. The mean absolute error amounts to 0.8 ppm and the standard deviation is 0.2 ppm. This confirms our previous studies on this approximation with the scalar DLU-X2C Hamiltonian.[116] Consequently, the snK approximation is well suited for 1c and 2c response equations.

Overall, the mean absolute error of the combined approximations is 0.8 ppm with a standard deviation of 0.7 ppm. Therefore, the DLU, RI-J, and snK approximations are well suited for NMR properties with one-component and two-component approaches. Among the three approximations, the DLU scheme introduces the smallest error.

C. Assessment of efficiency for a tin pincer ligand

Efficiency assessments were carried out for the tin pincer ligand **SnNSn** introduced in Ref. 181. This system consists of 107 atoms, featuring the sum formula $Sn_2N_7C_{39}H_{59}$. Using the x2c-TZVPPall-2c basis set, 2400 contracted basis functionals (spherical AO representation).

Figure 1 clearly shows the advantage of the seminumerical algorithms. Even for moderate grid sizes, the overall wall time is reduced by nearly an order of magnitude. Interestingly, while for analytical exact exchange solving the CPKS equations fully dominates the wall time, this is no longer true for seminumerical exchange. For the latter, the time spend to calculate the X2C contributions can become significant, especially if NMR shieldings are requested for many nuclei. Contrary, the CPKS equations are independent of the number of nuclei for which the NMR shieldings are to be calculated due to them only depending on the three Cartesian directions of the magnetic fields. Therefore, especially when combined with seminumerical exchange, it is advisable to limit investigations to the nuclei of interest. One-electron contributions such as the calculation of the perturbed overlap matrix or the magnetic-field derivative of the Hamiltonian account for no significant time in the overall calculation. It is further noted that the errors for the mean NMR shielding constant of the tin nuclei, found at 2585.71 for analytical HF exchange are offset by 2.02/0.77/0.66/ − 0.26 for the snK approach using the coarse/medium/fine/veryfine grids, respectively. This corresponds to deviations of 0.08% for the coarse grid and less than 0.03% in all other cases. These results are in line with the errors found in Sec. V B for medium-sized grids.

The isotropic NMR shielding constant of $SnMe_4$ amounts to 2412.6 ppm with analytical HF exchange, see Sec. V B. Thus, the chemical shift is around −173 ppm and consequently in reasonable agreement with the experimental finding of −136 ppm.[181]

The snK approximation drastically reduces the wall times while introducing negligible errors. Calculations for large systems with more than 100 atoms can be carried out in less than an hour and thus studies of large can be performed routinely.

D. Phosphorous NMR shifts of low-valent organometallic Ge, Sn, and Pb complexes

The complexes $[(\{SIDipp\}P)_2Sn]$, $[(\{SIDipp\}P)_2Pb]$, $[(\{SIDipp\}P)SnCl]_2$, and $[(\{SIDipp\}P)PbBr]_2$ are shown in Fig. 2 and were originally synthesized and characterized in

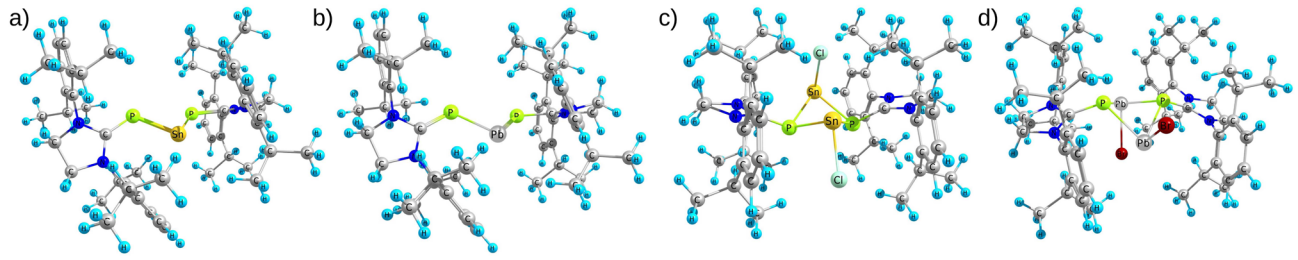

FIG. 2. Structures of (a) $[(\{SIDipp\}P)_2Sn]$, (b) $[(\{SIDipp\}P)_2Pb]$, (c) $[(\{SIDipp\}P)SnCl]_2$, and (d) $[(\{SIDipp\}P)PbCl]_2$, SIDipp = 1,3-bis(2,6-di-isopropylphenyl)-imidazolidin-2-ylidene. Structures are taken from Ref. 182 and were optimized with the scalar DLU-X2C Hamiltonian at the TPSS/x2c-TZVPall level of theory.

Ref. 182. The first two organometallic compounds feature P–M bonds (M = Sn, Pb) with notable p_π–p_π or double bond character.[182] The experimental M–P NMR coupling constants were recently reproduced by the DLU-X2C Hamiltonian in excellent agreement,[84,85] whereas the initial study of the ^{31}P NMR shifts in Ref. 182 did not yield accurate results for all compounds. Here, we complement the original studies with two-component NMR shifts. NMR shifts for [({SIDipp}P)$_2$Sn] and [({SIDipp}P)$_2$Pb] are listed in Table IV and those for [({SIDipp}P)SnCl]$_2$ and [({SIDipp}P)PbBr]$_2$ are displayed in Table V.

PH_3 is used as reference for ^{31}P NMR chemical shifts to avoid aqueous H_3PO_4 (85%). The two scales can be converted with the absolute shielding constants of 328.35 ppm for 85% aqueous H_3PO_4 and 594.45 ppm for PH_3 in the gas phase.[211] See supplementary material for the structures of PH_3 with the employed density functional approximations.

TABLE IV. Mean ^{31}P NMR chemical shift (in ppm) of [({SIDipp}P)$_2$Sn] and [({SIDipp}P)$_2$Pb] with the scalar (SR) and spin–orbit (SO) DLU-X2C Hamiltonians and various density functional approximations (SDFT for 2c calculations). The x2c-TZVPall-2c basis sets are applied throughout and the molecules consist of 137 atoms. Experimental results (Expt.) are taken from Ref. 182.

	[({SIDipp}P)$_2$Sn]		[({SIDipp}P)$_2$Pb]	
Method	SR	SO	SR	SO
BP86	203	174	222	158
PBE	187	159	203	141
TPSS	149	126	162	122
B3LYP	200	172	225	175
PBE0	139	113	149	104
TPSSh	141	118	141	107
CAM-B3LYP	160	130	139	100
Expt.	121.4		116.8	

TABLE V. Mean ^{31}P NMR chemical shift (in ppm) of [({SIDipp}P)SnCl]$_2$ and [({SIDipp}P)PbBr]$_2$ with the scalar (SR) and spin–orbit (SO) DLU-X2C Hamiltonians and various density functional approximations (SDFT for 2c calculations). The x2c-TZVPall-2c basis sets are applied throughout and the molecules consist of 140 atoms. Experimental results (Expt.) are taken from Ref. 182.

	[({SIDipp}P)SnCl]$_2$		[({SIDipp}P)PbBr]$_2$	
Method	SR	SO	SR	SO
BP86	−4	−26	5	−24
PBE	−8	−31	0	−34
TPSS	−42	−61	−33	−52
B3LYP	−13	−30	−10	−14
PBE0	−64	−83	−44	−55
TPSSh	−56	−74	−48	−61
CAM-B3LYP	−46	−62	−39	−35
Expt.	−66.2		−47.6	

For the monometallic complexes, spin–orbit interaction is of great importance for the NMR shifts, as the change amounts to almost 30 and 50 ppm for [({SIDipp}P)$_2$Sn] and [({SIDipp}P)$_2$Pb], respectively. The scalar-relativistic results substantial overestimation the NMR shifts, whereas the two-component calculations lead to a good agreement with the experimental findings. A notable exception in this regard are the B3LYP calculations, which still show a discrepancy of almost 50 ppm. Here, B3LYP performs worse than pure semilocal functional such as PBE or TPSS. The best agreement is found with TPSS followed by PBE0 and TPSSh, which lead to an error of about 10 ppm compared to the experiment. All density functionals considered herein were able to correctly predict the trend of a more positive NMR shift for [({SIDipp}P)$_2$Pb] compared to [({SIDipp}P)$_2$Sn]. Here, the admixture of HF exchange consistently lowers the NMR shifts. The rather good performance of PBE0 for Sn NMR shifts was also observed in a comprehensive benchmark study with the spin–orbit ZORA and the scalar X2C Hamiltonian.[42]

Concerning the computational demands, NMR shift calculations of [({SIDipp}P)$_2$Pb] with 2444 contracted basis functionals (spherical AO representation) take about 1.5 h for pure functionals (PBE, 7 iterations) and 16.9 h for hybrid functionals (PBE0, 13 iterations) using 12 OpenMP threads of an Intel Xeon Gold 6212U CPU (2.40 GHz, Intel Fortran Compiler 19.0.1.144). The wall time for the 2c SCF calculations amounts to 0.7 h (PBE, 35 iterations) and 5.2 h (PBE0, 51 iterations), respectively, based on converged 1c SCF solutions. To compare with, the 1c NMR shift calculations take 5.5 min (PBE, no iterations) and 1.1 h (PBE0, 8 iterations), while the 1c SCF procedure requires 20.5 min (PBE, 36 iterations) and 2.7 h (PBE0, 34 iterations) with a superposition of atomic densities based on Hückel AOs as initial guess.

The bimetallic compounds [({SIDipp}P)SnCl]$_2$ and [({SIDipp}P)PbBr]$_2$ feature a much smaller multibond M–P character and consequently decreased P NMR shifts[182] as shown in Table V. All calculations follow this qualitative trend. However, spin–orbit coupling does not always improve the results for the hybrid functionals. For TPSSh and PBE0 the 2c formalism slightly worsens the results hinting at (partial) error cancellation. Again, TPSS shows the smallest deviations of only 5 ppm. However, the trend from [({SIDipp}P)SnCl]$_2$ to [({SIDipp}P)PbBr]$_2$ is underestimated, as the calculated shift for the first is to small by 5 ppm and the second is to large by 5 ppm in (absolute values). Given that other functionals such as PBE even fail to reproduce the decrease of the shifts (in absolute values), TPSS is still a well suited and computationally cheap functional for the four complexes.

Overall, the spin–orbit DLU-X2C approach allows for the prediction of NMR shifts in very good agreement with experimental data using low-cost computer hardware.

E. Nucleus-independent chemical shifts of all-metal aromatic systems

The concept of aromaticity[212] and Hückel's $(4n + 2)$ rule[213–215] are typically introduced for organic compounds, with n denoting the number of cyclic delocalized π electrons. However, the concept is not restricted to organic molecules and a few so-called all-metal aromatic compounds were experimentally secured.[186–195] As aromaticity cannot simply be measured, a couple of criteria exist to

assess the degree of aromaticity and the respective electron delocalization.[216] A popular one is the magnetic criterion,[149–154] which makes use of Ampère's law and the resulting diatropic ring current leading to characteristic NMR shifts.[217] This ring current can be calculated directly, e.g., with the gauge-including magnetically induced currents (GIMIC) method,[218–221] or indirectly with NICS.[148] Alternatively, the ring current can be computed from the shielding tensor and a line integration according to the Ampère–Maxwell law.[222,223] Herein, we study the impact of spin–orbit coupling on all-metal aromatic systems with NICS. We note in passing that four-component methods were also used to assess the magnetically induced currents of various molecules,[224–226] however, a wider study on all-metal aromatic systems was not presented to the best of our knowledge. Scalar-relativistic and spin–orbit NICS are listed in Table VI for a selection[194] of all-metal aromatic and antiaromatic (sub-)systems. We refer to Ref. 194 for details on the selection.

First, the NICS calculations and the GIMIC results lead to a qualitative agreement for the scalar-relativistic calculations. That means, compounds are consistently classified as aromatic or antiaromatic. For small rings, NICS overestimate the ring current due to the small spatial distance of the NICS atom and the chemical bond.

Second, the impact of spin–orbit coupling is small for light elements, as expected. For compounds consisting of lighter elements than Kr, the NICS are changed by at most 0.3 ppm at the complete SDFT level. Starting with the next row of the periodic table, substantial changes in absolute numbers are observed. For instance, the NICS changes by about 6 ppm for In_4^{2-} or 3 ppm for Sn_5^{6-}. A drastic change is found for the antiaromatic system Bi_4^{2-}, as the NICS rises from 4.3 to 32.1 ppm. Overall, the impact of the XC kernel on the NICS is rather small for most systems. A notable exception in this regard is again Bi_4^{2-}, where the inclusion of the XC kernel changes the result by 6 ppm or more than 25%.

Results for Bi_6^{2-} and the related complexes $\mathbf{1}^-$ and $\mathbf{2}^-$ of Ref. 195 are listed in Table VII. Bi_6^{2-} features a non-localizable φ-type orbital and sustains a notable ring current based on GIMIC and NICS using scalar-relativistic effective core potentials, see Ref. 195 for details. Herein, we complement the scalar-relativistic results with spin–orbit X2C NICS calculations. The results in Table VII reveal a similar picture as the previous studies for the other metal compounds herein. Spin–orbit coupling leads to a minor decrease of the NICS but the qualitative assignment is not changed. Therefore, previous classifications remain unchanged and are further confirmed by the present study.

TABLE VI. NICS of all-metal aromatic compounds at the scalar x2c-TZVPall-s/PBE0 and spin–orbit x2c-TZVPall-2c/PBE0 levels. The corresponding DLU-X2C Hamiltonian and the RI-J approximation are employed. COSMO is applied for the charged systems. NICS are given in ppm. Sb_4^{2-} and Bi_4^{2-} are antiaromatic based on the magnetic criterion. Furthermore, ring current strengths (in nA/T) obtained with the gauge-including magnetically induced currents (GIMIC) method[218–221] for the SR DLU-X2C Hamiltonian are listed. Structures and placement of the NICS atom, i.e., NICS(0), are taken from previous work.[194] Scalar results for Bi_{12}^{8-} taken from Ref. 116. A negative value for NICS and a positive value for GIMIC indicate a diatropic or aromatic ring current.

	Scalar		Spin–Orbit	
Compound	GIMIC	NICS	DFT NICS	SDFT NICS
Sb_3^{3-}	15.7	−42.3	−40.6	−39.6
$(AlH)_3^{2-}$	3.9	−19.4	−19.3	−19.4
$(GaH)_3^{2-}$	5.5	−17.9	−17.8	−17.8
Al_4^{2-}	27.9	−34.4	−34.2	−34.1
Ga_4^{2-}	32.8	−36.1	−34.8	−36.1
In_4^{2-}	33.2	−33.1	−27.3	−26.2
$(Ga(CH_3))_2Ga_2^{2-}$	23.3	−23.0	−22.6	−22.5
Sb_4^{2-}	−4.7	3.3	7.2	8.0
Bi_4^{2-}	−5.6	4.3	26.3	32.1
Hg_4^{6-}	33.6	−28.6	−22.8	−20.9
Ge_5^{6-}	34.7	−27.6	−27.5	−27.5
Sn_5^{6-}	31.1	−17.5	−15.0	−14.8
Pb_5^{6-}	34.7	−21.5	−14.7	−12.0
Sb_5^-	16.2	−11.3	−10.4	−9.8
Bi_5^-	14.5	−9.5	−11.7	−8.9
Bi_{12}^{8-}	22.3	−17.3	−13.2	−11.7

TABLE VII. NICS (in ppm) at the SR and SO SDFT levels for Bi_6^{2-}, $\mathbf{1}^-$, and $\mathbf{2}^-$. The x2c-TZVPall-s basis set is applied with the TPSS functional and COSMO. CMS denotes the global center of mass. NICS(y) (y = 0, 1, 2, 3) are further listed, with y denoting the distance above the upper Bi_3 triangle in bohr. The DLU scheme and the finite nucleus model are applied throughout. SO X2C calculations further apply the modified screened-nuclear spin–orbit (mSNSO) correction. Structures are taken from Ref. 195.

	Bi_6^{2-}		$\mathbf{1}^-$		$\mathbf{2}^-$	
NICS	SR	SO	SR	SO	SR	SO
NICS(CMS)	−36.1	−31.0	−22.2	−14.0	−29.6	−22.9
NICS(0)	−55.3	−46.5	−45.6	−37.3	−48.1	−42.0
NICS(1)	−48.7	−39.4	−42.4	−36.9	−41.6	−37.3
NICS(2)	−31.7	−22.2	−27.4	−23.6	−25.8	−22.2
NICS(3)	−15.7	−9.2	−13.4	−10.9	−12.3	−9.9

VI. SUMMARY AND CONCLUSIONS

We presented an efficient formulation of exact two-component (X2C) theory for NMR shifts in a modern density functional framework up to the class of range-separated hybrid functionals. Efficiency is ensured by the diagonal local approximation to the unitary decoupling transformation (DLU), the (multipole-accelerated) resolution of the identity approximation for the Coulomb term (MARI-J, RI-J), and the seminumerical exchange (snK) approximation. The errors introduced by these approximations were assessed for a set of small tin compounds and found to be negligible. Among the three approximations, DLU introduces the smallest error of at most 0.2 ppm for chemical shifts in a range of almost 3000 ppm. To compare with, spin–orbit effects on the NMR shifts lead to changes of about 1000 ppm for a few compounds.

The accuracy of the X2C Hamiltonian was studied for the halogen halides molecules in comparison to four-component Dirac–Kohn–Sham approaches. Even for HAt with very pronounced spin–orbit effects the deviation amounts to less than 5% for the S-VWN, BP86, KT2, and B3LYP density functional approx-

imations. Compared to the four-component ansatz, X2C comes with reduced computational demands and the applicability to large organometallic systems was demonstrated for phosphorous NMR shifts of the low-valent Sn and Pb complexes synthesized and characterized in Ref. 182. Here, an excellent agreement of theory and experiment was reached with the TPSS functional. Furthermore, timings were presented for a tin pincer-type ligand[181] demonstrating that two-component NMR calculations of large molecules featuring about 2400 basis functions can be carried out in less than 1 h.

Finally, the impact of spin–orbit coupling on all-metal aromatic systems was assessed with the nucleus-independent chemical shift (NICS) formalism, where spin–orbit effects lead to a decrease of the ring current strength.

Future work will address the development of tailored basis sets[172,209,227,228] for spin–orbit NMR shieldings and the current-dependent generalization of the kinetic-energy density τ.[68] One the one hand, a first version of tailored basis sets can be constructed by combing the extensions of the x2c-XVP-s (X = S, TZ) basis sets[172] with the 2c patches[229] of the x2c-type basis sets[179] and removing linear dependencies. The respective quadruple-ζ x2c-QZVPall-2c-s basis sets were already presented in Ref. 209, as these follow a slightly different construction scheme. On the other hand, the current-dependent generalization of the kinetic-energy density will lead to non-linear effects for the magnetic-field response contribution. Spin–orbit coupling induces a current density in the ground state which will interact with the current density induced by the magnetic field.[68,230]

SUPPLEMENTARY MATERIAL

Supplementary material is available with the structures optimized in this work (txt file), coordinates of H_2Te (same txt file), and complete data for NMR shieldings and shifts of Secs. V A–V D (xlsx file).

ACKNOWLEDGMENTS

We thank Florian Weigend and Florian Bruder (Marburg) for fruitful discussions and encouraging comments. Y.J.F. acknowledges financial support by Turbomole GmbH. Most routines were developed while he was supported through a fellowship by Fonds der Chemischen Industrie (FCI, German Chemical Industry Funds). This work used computer hardware funded by FCI. C.H. gratefully acknowledges funding by the Volkswagen Foundation.

AUTHOR DECLARATIONS

Conflict of Interest

The authors have no conflicts to disclose.

Author Contributions

Yannick J. Franzke: Conceptualization (lead); Data curation (lead); Formal analysis (lead); Investigation (lead); Methodology (lead); Software (lead); Validation (equal); Visualization (supporting); Writing – original draft (lead); Writing – review & editing (lead). **Christof Holzer**: Conceptualization (supporting); Data curation (supporting); Formal analysis (supporting); Investigation (supporting); Methodology (supporting); Software (supporting); Validation (equal); Visualization (lead); Writing – original draft (supporting); Writing – review & editing (supporting).

DATA AVAILABILITY

The data that support the findings of this study are available within the article and its supplementary material.

APPENDIX A: DERIVATIVES OF THE RENORMALIZATION MATRIX

Derivatives of the renormalization matrix $\mathbf{R}$ are obtained by differentiating the relation[100]

$$\boldsymbol{R}\boldsymbol{R} = \tilde{\boldsymbol{S}}^{-1}\boldsymbol{S}. \tag{A1}$$

This leads to the Sylvester matrix equations

$$\boldsymbol{R}\boldsymbol{R}^{\lambda} + \boldsymbol{R}^{\lambda}\boldsymbol{R} = \boldsymbol{Q}^{\lambda}, \tag{A2}$$

where λ indicates the specific perturbation (B or m). The index of the Cartesian component (u, w) and the specific nucleus (I) will be dropped for simplicity.

For the magnetic-field derivative the right-hand side is given by

$$\mathbf{Q}^{B} = \tilde{\mathbf{S}}^{-1}\left(\mathbf{S}^{B} - \tilde{\mathbf{S}}^{B}\mathbf{R}\mathbf{R}\right). \tag{A3}$$

For the derivatives with respect to the magnetic moments, it follows as

$$\mathbf{Q}^{m} = -\tilde{\mathbf{S}}^{-1}\tilde{\mathbf{S}}^{m}\mathbf{R}\mathbf{R}. \tag{A4}$$

For the second-order derivatives the Sylvester equation to be solved reads

$$\boldsymbol{R}\,\boldsymbol{R}^{Bm} + \boldsymbol{R}^{Bm}\,\boldsymbol{R} = \boldsymbol{Q}^{Bm} \tag{A5}$$

with the right-hand side

$$\begin{aligned}\mathbf{Q}^{Bm} = \tilde{\mathbf{S}}^{-1}\big[&-\tilde{\mathbf{S}}^{Bm}\mathbf{R}\mathbf{R} + \tilde{\mathbf{S}}^{B}\tilde{\mathbf{S}}^{-1}\tilde{\mathbf{S}}^{m}\mathbf{R}\mathbf{R}\\ &+ \tilde{\mathbf{S}}^{m}\tilde{\mathbf{S}}^{-1}\left(\tilde{\mathbf{S}}^{B}\mathbf{R}\mathbf{R} - \mathbf{S}^{B}\right)\big] - \mathbf{R}^{B}\mathbf{R}^{m} - \mathbf{R}^{m}\mathbf{R}^{B}.\end{aligned} \tag{A6}$$

These equations can be solved with an eigenvalue decomposition method, see Refs. 79 or 84. Note that the derivatives of $\tilde{\mathbf{S}}$ require the derivatives of the decoupling matrix $\mathbf{X}$ according to

$$\tilde{\mathbf{S}}^{B} = \mathbf{S}^{B} + \frac{1}{2c^2}\left(\mathbf{X}^{\dagger,B}\mathbf{T}\mathbf{X} + \mathbf{X}^{\dagger}\mathbf{T}^{B}\mathbf{X} + \mathbf{X}^{\dagger}\mathbf{T}\mathbf{X}^{B}\right) \tag{A7}$$

$$\tilde{\mathbf{S}}^{m} = \frac{1}{2c^2}\left(\mathbf{X}^{\dagger,m}\mathbf{T}\mathbf{X} + \mathbf{X}^{\dagger}\mathbf{T}\mathbf{X}^{m}\right) \tag{A8}$$

for the first-order derivatives and similar for second-order derivatives based on the product rule

$$\begin{aligned}\tilde{\mathbf{S}}^{Bm} = &\frac{1}{2c^2}\left(\mathbf{X}^{\dagger,Bm}\mathbf{T}\mathbf{X} + \mathbf{X}^{\dagger}\mathbf{T}\mathbf{X}^{Bm}\right)\\ &+ \frac{1}{2c^2}\left(\mathbf{X}^{\dagger,m}\mathbf{T}^{B}\mathbf{X} + \mathbf{X}^{\dagger,m}\mathbf{T}\mathbf{X}^{B} + \mathbf{X}^{\dagger,B}\mathbf{T}\mathbf{X}^{m}\right).\end{aligned} \tag{A9}$$

In DLU, we only have to solve these Sylvester equations for the atomic diagonal blocks.

APPENDIX B: DERIVATIVES OF THE DECOUPLING MATRIX

The derivatives of the decoupling matrix necessitate the perturbed coefficients $\mathbf{C}^{\mathrm{L}}, \mathbf{C}^{\mathrm{S}}$. The one-electron four-component Dirac equation in a matrix form is of the same structure as the Roothaan–Hall equations[231,232]

$$\mathbb{D}\mathbb{C} = \mathbb{M}\mathbb{C}\mathbb{E}. \tag{B1}$$

$\mathbb{D}$ and $\mathbb{M}$ are the four-component Dirac matrix and the respective metric. $\mathbb{C}$ and $\mathbb{E}$ denote the respective coefficients and energy eigenvalues. In detail, Eq. (B1) reads

$$\begin{pmatrix} \mathbf{V} & \mathbf{\Pi}^{\dagger} \\ \mathbf{\Pi} & \left(\frac{1}{4c^2}\mathbf{W} - \mathbf{T}\right) \end{pmatrix} \begin{pmatrix} \mathbf{C}_{-}^{\mathrm{L}} & \mathbf{C}_{+}^{\mathrm{L}} \\ \mathbf{C}_{-}^{\mathrm{S}} & \mathbf{C}_{+}^{\mathrm{S}} \end{pmatrix} = \begin{pmatrix} \mathbf{S} & \mathbf{0}_2 \\ \mathbf{0}_2 & \frac{1}{2c^2}\mathbf{T} \end{pmatrix} \begin{pmatrix} \mathbf{C}_{-}^{\mathrm{L}} & \mathbf{C}_{+}^{\mathrm{L}} \\ \mathbf{C}_{-}^{\mathrm{S}} & \mathbf{C}_{+}^{\mathrm{S}} \end{pmatrix} \times \begin{pmatrix} \mathbf{E}_{-} & \mathbf{0}_2 \\ \mathbf{0}_2 & \mathbf{E}_{+} \end{pmatrix} \tag{B2}$$

where $\mathbf{\Pi}$ equals $\mathbf{T}$ in the limit of vanishing perturbations. $\pm$ indicate the positive-energy ("electronic") and negative-energy ("positronic") states. Considering the similarities of the Dirac and the Roothaan-Hall equation, the perturbed coefficients are obtained with the orbital rotations

$$\mathbb{C}^{\lambda} = \mathbb{C}\mathbb{U}^{\lambda}, \tag{B3}$$

$$\mathbb{C}^{Bm} = \mathbb{C}\left[\mathbb{U}^{Bm} + \mathbb{U}^{B}\mathbb{U}^{m}\right] = \mathbb{C}\tilde{\mathbb{U}}^{Bm}, \tag{B4}$$

where $\lambda = B, m$. Then, the first-order derivative of the decoupling matrix follows as

$$\boldsymbol{X}^{\lambda} = \left(\boldsymbol{C}_{-}^{S} - \boldsymbol{X}\boldsymbol{C}_{-}^{L}\right) \boldsymbol{U}_{-+}^{\lambda} \, \boldsymbol{C}_{+}^{L,\dagger} \, \tilde{\boldsymbol{S}}. \tag{B5}$$

Thus, only the positronic-electronic block is needed for $\boldsymbol{X}^{\lambda}$. However, more blocks of the first-order rotation matrix are needed for the second-order derivative

$$\boldsymbol{X}^{B,m} = (\boldsymbol{C}_{S-} - \boldsymbol{X}\boldsymbol{C}_{L-})\Big[\tilde{\boldsymbol{U}}_{-+}^{B,m} - \boldsymbol{U}_{-+}^{m} \, \boldsymbol{U}_{++}^{B} - \boldsymbol{U}_{-+}^{B} \, \boldsymbol{C}_{L+}^{\dagger} \times \tilde{\boldsymbol{S}} \, \boldsymbol{C}_{L-} \, \boldsymbol{U}_{-+}^{m} - \boldsymbol{U}_{-+}^{m} \, \boldsymbol{C}_{L+}^{\dagger} \, \tilde{\boldsymbol{S}} \, \boldsymbol{C}_{L-} \, \boldsymbol{U}_{-+}^{B}\Big] \, \boldsymbol{C}_{L+}^{\dagger} \, \tilde{\boldsymbol{S}}. \tag{B6}$$

For the magnetic-field derivatives the respective blocks of the first-order orbital rotation matrix are given by

$$(\mathbf{U}_{--}^{B})_{kl} = -\frac{1}{2}(\tilde{\mathbf{M}}_{--}^{B})_{kl}, \tag{B7}$$

$$(\mathbf{U}_{-+}^{B})_{kl} = \frac{(\tilde{\mathbf{D}}_{-+}^{B})_{kl} - (\tilde{\mathbf{M}}_{u,-+}^{B})_{kl} \, (\mathbf{E}_{++})_{ll}}{(\mathbf{E}_{++})_{ll} - (\mathbf{E}_{--})_{kk}}, \tag{B8}$$

$$(\mathbf{U}_{+-}^{B})_{kl} = \frac{(\tilde{\mathbf{D}}_{+-}^{B})_{kl} - (\tilde{\mathbf{M}}_{+-}^{B})_{kl} \, (\mathbf{E}_{--})_{ll}}{(\mathbf{E}_{--})_{ll} - (\mathbf{E}_{++})_{kk}}, \tag{B9}$$

$$(\mathbf{U}_{++}^{B})_{kl} = -\frac{1}{2}(\tilde{\mathbf{M}}_{++}^{B})_{kl}. \tag{B10}$$

Here, the tilde indicates that the basis of the unperturbed solutions is used, i.e., $\tilde{\mathbb{D}}^{B} = \mathbb{C}^{\dagger}\mathbb{D}^{B}\mathbb{C}$. The indices k, l refer to the states of the corresponding block ($--$, $-+$, $+-$, $++$). The derivatives of the metric only arise due to the GIAOs. Similarly, the magnetic-moment derivative part is calculated as

$$(\mathbf{U}_{--}^{m})_{kl} = \mathbf{0}_2, \tag{B11}$$

$$(\mathbf{U}_{-+}^{m})_{kl} = \frac{(\tilde{\mathbf{D}}_{-+}^{m})_{kl}}{(\mathbf{E}_{++})_{ll} - (\mathbf{E}_{--})_{kk}}, \tag{B12}$$

$$(\mathbf{U}_{+-}^{m})_{kl} = \frac{(\tilde{\mathbf{D}}_{+-}^{m})_{kl}}{(\mathbf{E}_{--})_{ll} - (\mathbf{E}_{++})_{kk}}, \tag{B13}$$

$$(\mathbf{U}_{++}^{m})_{kl} = \mathbf{0}_2. \tag{B14}$$

The derivatives of the metric and consequently the orbital rotation of the $--$ and $++$ blocks vanish, as the basis functions are independent of m.

The positronic-electronic block of the second-order orbital rotation matrix for NMR shifts reads

$$\begin{aligned}(\tilde{\mathbf{U}}_{-+}^{B,m})_{kl} = \frac{1}{(\mathbf{E}_{++})_{ll} - (\mathbf{E}_{--})_{kk}} \Big\{ &(\tilde{\mathbf{D}}_{-+}^{B,m})_{kl} + \left(\mathbf{U}_{-+}^{m}\mathbf{U}_{++}^{B} + \mathbf{U}_{--}^{B}\mathbf{U}_{-+}^{m}\right)_{kl} \\ &\times (\mathbf{E}_{++})_{ll} - \left(\mathbf{U}_{-+}^{m}\mathbf{E}_{++}\mathbf{U}_{++}^{B} + \mathbf{U}_{--}^{B}\mathbf{E}_{--}\mathbf{U}_{-+}^{m}\right)_{kl} \\ &+ \left[\mathbf{U}_{+-}^{\dagger,m}\left((\tilde{\mathbf{D}}_{++}^{B}) - (\tilde{\mathbf{M}}_{++}^{B})(\mathbf{E}_{++})\right)\right]_{kl} + \left[\left(\tilde{\mathbf{D}}_{--}^{B} - \tilde{\mathbf{M}}_{--}^{B}\mathbf{E}_{--}\right)\mathbf{U}_{-+}^{m}\right]_{kl} \\ &+ \left[\mathbf{U}_{--}^{\dagger,B}(\tilde{\mathbf{D}}_{-+}^{m})\right]_{kl} + \left[\tilde{\mathbf{D}}_{-+}^{m}\mathbf{U}_{++}^{B}\right]_{kl}\Big\}. \end{aligned} \tag{B15}$$

In DLU, only the atomic diagonal blocks of the decoupling matrix are needed and therefore only the atomic diagonal blocks of the orbital rotations are calculated.

REFERENCES

[1] T. Helgaker, M. Jaszuński, and K. Ruud, Chem. Rev. **99**, 293 (1999).
[2] *Calculation of NMR and EPR Parameters. Theory and Applications*, edited by M. Kaupp, M. Bühl, and V. G. Malkin (Wiley VCH, Weinheim, Germany, 2004).
[3] J. Vaara, Phys. Chem. Chem. Phys. **9**, 5399 (2007).
[4] T. Nakajima and K. Hirao, Chem. Rev. **112**, 385 (2012).
[5] P. Pyykkö, Annu. Rev. Phys. Chem. **63**, 45 (2012).
[6] J. Autschbach, J. Chem. Phys. **136**, 150902 (2012).
[7] J. Autschbach, Philos. Trans. R. Soc., A **372**, 20120489 (2014).
[8] M. Repisky, S. Komorovsky, R. Bast, and K. Ruud, *Gas Phase NMR*, edited by K. Jackowski and M. Jaszuński (The Royal Society of Chemistry, Cambridge, United Kingdom, 2016), Chap. 8, pp. 267–303.
[9] C. Chang, M. Pelissier, and P. Durand, Phys. Scr. **34**, 394 (1986).
[10] E. van Lenthe, E. J. Baerends, and J. G. Snijders, J. Chem. Phys. **99**, 4597 (1993).
[11] E. van Lenthe, E. J. Baerends, and J. G. Snijders, J. Chem. Phys. **101**, 9783 (1994).
[12] W. Kutzelnigg and W. Liu, J. Chem. Phys. **123**, 241102 (2005).
[13] W. Liu and W. Kutzelnigg, J. Chem. Phys. **126**, 114107 (2007).
[14] W. Liu and D. Peng, J. Chem. Phys. **125**, 044102 (2006).
[15] W. Liu and D. Peng, J. Chem. Phys. **125**, 149901 (2006).
[16] M. Iliaš and T. Saue, J. Chem. Phys. **126**, 064102 (2007).
[17] D. Peng, W. Liu, Y. Xiao, and L. Cheng, J. Chem. Phys. **127**, 104106 (2007).
[18] W. Liu and D. Peng, J. Chem. Phys. **131**, 031104 (2009).
[19] T. Saue, ChemPhysChem **12**, 3077 (2011).
[20] W. Liu, J. Chem. Phys. **152**, 180901 (2020).

[21] S. Komorovský, M. Repiský, O. L. Malkina, V. G. Malkin, I. Malkin Ondík, and M. Kaupp, J. Chem. Phys. **128**, 104101 (2008).
[22] S. Komorovský, M. Repiský, O. L. Malkina, and V. G. Malkin, J. Chem. Phys. **132**, 154101 (2010).
[23] Y. Xiao, W. Liu, L. Cheng, and D. Peng, J. Chem. Phys. **126**, 214101 (2007).
[24] Y. Xiao, D. Peng, and W. Liu, J. Chem. Phys. **126**, 081101 (2007).
[25] L. Cheng, Y. Xiao, and W. Liu, J. Chem. Phys. **131**, 244113 (2009).
[26] Y. Xiao, Q. Sun, and W. Liu, Theor. Chem. Acc. **131**, 1080 (2012).
[27] G. A. Aucar, T. Saue, L. Visscher, and H. J. A. Jensen, J. Chem. Phys. **110**, 6208 (1999).
[28] M. Iliaš, T. Saue, T. Enevoldsen, and H. J. A. Jensen, J. Chem. Phys. **131**, 124119 (2009).
[29] M. Olejniczak, R. Bast, T. Saue, and M. Pecul, J. Chem. Phys. **136**, 014108 (2012).
[30] M. Olejniczak, R. Bast, T. Saue, and M. Pecul, J. Chem. Phys. **136**, 239902 (2012).
[31] F. London, J. Phys. Radium **8**, 397 (1937).
[32] R. Ditchfield, Mol. Phys. **27**, 789 (1974).
[33] L. Cheng, J. Gauss, and J. F. Stanton, J. Chem. Phys. **139**, 054105 (2013).
[34] Y. J. Franzke and F. Weigend, J. Chem. Theory Comput. **15**, 1028 (2019).
[35] T. Yoshizawa, W. Zou, and D. Cremer, J. Chem. Phys. **146**, 134109 (2017).
[36] T. Yoshizawa and M. Hada, J. Chem. Phys. **147**, 154104 (2017).
[37] Q. Sun, W. Liu, Y. Xiao, and L. Cheng, J. Chem. Phys. **131**, 081101 (2009).
[38] Q. Sun, Y. Xiao, and W. Liu, J. Chem. Phys. **137**, 174105 (2012).
[39] S. K. Wolff, T. Ziegler, E. van Lenthe, and E. J. Baerends, J. Chem. Phys. **110**, 7689 (1999).
[40] M. Krykunov, T. Ziegler, and E. van Lenthe, J. Phys. Chem. A **113**, 11495 (2009).
[41] J. Autschbach, Mol. Phys. **111**, 2544 (2013).
[42] J. B. Stückrath, T. Gasevic, M. Bursch, and S. Grimme, Inorg. Chem. **61**, 3903 (2022).
[43] J. Vícha, J. Novotný, S. Komorovsky, M. Straka, M. Kaupp, and R. Marek, Chem. Rev. **120**, 7065 (2020).
[44] S. Halbert, C. Copéret, C. Raynaud, and O. Eisenstein, J. Am. Chem. Soc. **138**, 2261 (2016).
[45] A. H. Greif, P. Hrobárik, and M. Kaupp, Chem. Eur. J. **23**, 9790 (2017).
[46] K. P. Kornecki, J. F. Briones, V. Boyarskikh, F. Fullilove, J. Autschbach, K. E. Schrote, K. M. Lancaster, H. M. L. Davies, and J. F. Berry, Science **342**, 351 (2013).
[47] F. Alkan, S. T. Holmes, R. J. Iuliucci, K. T. Mueller, and C. Dybowski, Phys. Chem. Chem. Phys. **18**, 18914 (2016).
[48] D. E. Smiles, G. Wu, P. Hrobárik, and T. W. Hayton, J. Am. Chem. Soc. **138**, 814 (2016).
[49] J. Du, J. A. Seed, V. E. Berryman, N. Kaltsoyannis, R. W. Adams, D. Lee, and S. T. Liddle, Nat. Commun. **12**, 5649 (2021).
[50] G. T. Kent, X. Yu, G. Wu, J. Autschbach, and T. W. Hayton, Chem. Sci. **12**, 14383 (2021).
[51] A. M. Teale, O. B. Lutnæs, T. Helgaker, D. J. Tozer, and J. Gauss, J. Chem. Phys. **138**, 024111 (2013).
[52] R. Laskowski, P. Blaha, and F. Tran, Phys. Rev. B **87**, 195130 (2013).
[53] G. L. Stoychev, A. A. Auer, R. Izsák, and F. Neese, J. Chem. Theory Comput. **14**, 619 (2018).
[54] C. J. Schattenberg and M. Kaupp, J. Chem. Theory Comput. **17**, 7602 (2021).
[55] E. J. Baerends, D. E. Ellis, and P. Ros, Chem. Phys. **2**, 41 (1973).
[56] K. Eichkorn, O. Treutler, H. Öhm, M. Häser, and R. Ahlrichs, Chem. Phys. Lett. **240**, 283 (1995).
[57] K. Eichkorn, F. Weigend, O. Treutler, and R. Ahlrichs, Theor. Chem. Acc. **97**, 119 (1997).
[58] R. A. Friesner, Chem. Phys. Lett. **116**, 39 (1985).
[59] R. A. Friesner, J. Chem. Phys. **85**, 1462 (1986).
[60] R. A. Friesner, J. Chem. Phys. **86**, 3522 (1987).
[61] F. Neese, F. Wennmohs, A. Hansen, and U. Becker, Chem. Phys. **356**, 98 (2009).
[62] P. Plessow and F. Weigend, J. Comput. Chem. **33**, 810 (2012).
[63] C. Holzer, J. Chem. Phys. **153**, 184115 (2020).
[64] M. Gell-Mann, Nuovo Cimento **4**, 848 (1956).
[65] A. Bohr and V. F. Weisskopf, Phys. Rev. **77**, 94 (1950).
[66] A. C. Hennum, W. Klopper, and T. Helgaker, J. Chem. Phys. **115**, 7356 (2001).
[67] L. Visscher and K. G. Dyall, At. Data Nucl. Data Tables **67**, 207 (1997).
[68] C. Holzer, Y. J. Franzke, and A. Pausch, J. Chem. Phys. **157**, 204102 (2022).
[69] K. Wolinski, J. F. Hinton, and P. Pulay, J. Am. Chem. Soc. **112**, 8251 (1990).
[70] J. R. Cheeseman, G. W. Trucks, T. A. Keith, and M. J. Frisch, J. Chem. Phys. **104**, 5497 (1996).
[71] R. M. Stevens, R. M. Pitzer, and W. N. Lipscomb, J. Chem. Phys. **38**, 550 (1963).
[72] S. F. O'Shea and D. P. Santry, Theor. Chim. Acta **37**, 1 (1975).
[73] N. C. Handy and H. F. Schaefer, J. Chem. Phys. **81**, 5031 (1984).
[74] N. C. Handy, D. J. Tozer, G. J. Laming, C. W. Murray, and R. D. Amos, Isr. J. Chem. **33**, 331 (1993).
[75] B. G. Johnson and M. J. Fisch, J. Chem. Phys. **100**, 7429 (1994).
[76] L. Cheng and J. Gauss, J. Chem. Phys. **135**, 084114 (2011).
[77] L. Cheng and J. Gauss, J. Chem. Phys. **135**, 244104 (2011).
[78] W. Zou, M. Filatov, and D. Cremer, J. Chem. Phys. **134**, 244117 (2011).
[79] W. Zou, M. Filatov, and D. Cremer, J. Chem. Theory Comput. **8**, 2617 (2012).
[80] W. Zou, M. Filatov, and D. Cremer, J. Chem. Phys. **142**, 214106 (2015).
[81] Y. J. Franzke, N. Middendorf, and F. Weigend, J. Chem. Phys. **148**, 104110 (2018).
[82] W. Zou, G. Guo, B. Suo, and W. Liu, J. Chem. Theory Comput. **16**, 1541 (2020).
[83] T. Yoshizawa, Chem. Phys. **518**, 112 (2019).
[84] Y. J. Franzke, F. Mack, and F. Weigend, J. Chem. Theory Comput. **17**, 3974 (2021).
[85] Y. J. Franzke, J. Chem. Theory Comput. **19**, 2010 (2023).
[86] M. Filatov, W. Zou, and D. Cremer, J. Phys. Chem. A **116**, 3481 (2012).
[87] M. Filatov, W. Zou, and D. Cremer, J. Chem. Theory Comput. **8**, 875 (2012).
[88] T. Yoshizawa, W. Zou, and D. Cremer, J. Chem. Phys. **145**, 184104 (2016).
[89] T. Yoshizawa, M. Filatov, D. Cremer, and W. Zou, Mol. Phys. **117**, 1164 (2019).
[90] H. Zhu, C. Gao, M. Filatov, and W. Zou, Phys. Chem. Chem. Phys. **22**, 26776 (2020).
[91] Y. J. Franzke and J. M. Yu, J. Chem. Theory Comput. **18**, 2246 (2022).
[92] J. C. Boettger, Phys. Rev. B **62**, 7809 (2000).
[93] M. Filatov, W. Zou, and D. Cremer, J. Chem. Phys. **139**, 014106 (2013).
[94] A. Wodyński and M. Kaupp, J. Phys. Chem. A **123**, 5660 (2019).
[95] Y. J. Franzke and J. M. Yu, J. Chem. Theory Comput. **18**, 323 (2022).
[96] D. Peng, N. Middendorf, F. Weigend, and M. Reiher, J. Chem. Phys. **138**, 184105 (2013).
[97] K. G. Dyall, J. Chem. Phys. **106**, 9618 (1997).
[98] K. G. Dyall, J. Chem. Phys. **109**, 4201 (1998).
[99] K. G. Dyall and T. Enevoldsen, J. Chem. Phys. **111**, 10000 (1999).
[100] K. G. Dyall, J. Chem. Phys. **115**, 9136 (2001).
[101] D. Cremer, W. Zou, and M. Filatov, Wiley Interdiscip. Rev.: Comput. Mol. Sci. **4**, 436 (2014).
[102] Y. J. Franzke, "Calculation of NMR parameters in a modern relativistic density functional framework: Theory, implementation, and application," Dr. rer. nat. dissertation (Karlsruhe Institute of Technology (KIT), Germany, 2021).
[103] T. Zhang, J. M. Kasper, and X. Li, "Localized relativistic two-component methods for ground and excited state calculations," in *Annual Reports in Computational Chemistry*, edited by D. A. Dixon (Elsevier, Amsterdam, The Netherlands, 2020), Vol. 16, Chap. 2, pp. 17–37.
[104] D. Peng and M. Reiher, J. Chem. Phys. **136**, 244108 (2012).
[105] M. E. Casida, J. Mol. Struct.: THEOCHEM **914**, 3 (2009).
[106] J. Gao, W. Zou, W. Liu, Y. Xiao, D. Peng, B. Song, and C. Liu, J. Chem. Phys. **123**, 054102 (2005).
[107] F. Wang, T. Ziegler, E. van Lenthe, S. van Gisbergen, and E. J. Baerends, J. Chem. Phys. **122**, 204103 (2005).
[108] M. Kehry, Y. J. Franzke, C. Holzer, and W. Klopper, Mol. Phys. **118**, e1755064 (2020).
[109] S. N. Maximoff and G. E. Scuseria, Chem. Phys. Lett. **390**, 408 (2004).
[110] K. Reiter, F. Mack, and F. Weigend, J. Chem.Theory Comput. **14**, 191 (2018).
[111] C. J. Schattenberg and M. Kaupp, J. Chem. Theory Comput. **17**, 1469 (2021).
[112] J. F. Dobson, J. Chem. Phys. **98**, 8870 (1993).
[113] A. D. Becke, J. Chem. Phys. **117**, 6935 (2002).
[114] J. Tao, Phys. Rev. B **71**, 205107 (2005).

[115]J. E. Bates and F. Furche, J. Chem. Phys. **137**, 164105 (2012).
[116]C. Holzer, Y. J. Franzke, and M. Kehry, J. Chem. Theory Comput. **17**, 2928 (2021).
[117]Y. J. Franzke, C. Holzer, and F. Mack, J. Chem. Theory Comput. **18**, 1030 (2022).
[118]Y. J. Franzke and C. Holzer, J. Chem. Phys. **157**, 031102 (2022).
[119]R. Grotjahn, F. Furche, and M. Kaupp, J. Chem. Phys. **157**, 111102 (2022).
[120]F. Bruder, Y. J. Franzke, and F. Weigend, J. Phys. Chem. A **126**, 5050 (2022).
[121]J. Tao, J. P. Perdew, V. N. Staroverov, and G. E. Scuseria, Phys. Rev. Lett. **91**, 146401 (2003).
[122]J. Tao and Y. Mo, Phys. Rev. Lett. **117**, 073001 (2016).
[123]Y. Zhao and D. G. Truhlar, J. Chem. Phys. **125**, 194101 (2006).
[124]Y. Zhao and D. G. Truhlar, Theor. Chem. Acc. **120**, 215 (2008).
[125]T. Aschebrock and S. Kümmel, Phys. Rev. Res. **1**, 033082 (2019).
[126]J. Sun, A. Ruzsinszky, and J. P. Perdew, Phys. Rev. Lett. **115**, 036402 (2015).
[127]J. W. Furness, A. D. Kaplan, J. Ning, J. P. Perdew, and J. Sun, J. Phys. Chem. Lett. **11**, 8208 (2020).
[128]J. W. Furness, A. D. Kaplan, J. Ning, J. P. Perdew, and J. Sun, J. Phys. Chem. Lett. **11**, 9248 (2020).
[129]Manual of ADF 2023.1, see https://www.scm.com/doc/ADF/Input/NMR_chemical_shifts.html (retrieved July 30, 2023).
[130]R. Ahlrichs, M. Bär, M. Häser, H. Horn, and C. Kölmel, Chem. Phys. Lett. **162**, 165 (1989).
[131]S. G. Balasubramani, G. P. Chen, S. Coriani, M. Diedenhofen, M. S. Frank, Y. J. Franzke, F. Furche, R. Grotjahn, M. E. Harding, C. Hättig, A. Hellweg, B. Helmich-Paris, C. Holzer, U. Huniar, M. Kaupp, A. Marefat Khah, S. Karbalaei Khani, T. Müller, F. Mack, B. D. Nguyen, S. M. Parker, E. Perlt, D. Rappoport, K. Reiter, S. Roy, M. Rückert, G. Schmitz, M. Sierka, E. Tapavicza, D. P. Tew, C. van Wüllen, V. K. Voora, F. Weigend, A. Wodyński, and J. M. Yu, J. Chem. Phys. **152**, 184107 (2020).
[132]Y. J. Franzke, C. Holzer, J. H. Andersen, T. Begušić, F. Bruder, S. Coriani, F. Della Sala, E. Fabiano, D. A. Fedotov, S. Fürst, S. Gillhuber, R. Grotjahn, M. Kaupp, M. Kehry, M. Krstić, F. Mack, S. Majumdar, B. D. Nguyen, S. M. Parker, F. Pauly, A. Pausch, E. Perlt, G. S. Phun, A. Rajabi, D. Rappoport, B. Samal, T. Schrader, M. Sharma, E. Tapavicza, R. S. Treß, V. Voora, A. Wodyński, J. M. Yu, B. Zerulla, F. Furche, C. Hättig, M. Sierka, D. P. Tew, and F. Weigend, J. Chem. Theory Comput. (published online, 2023).
[133]TURBOMOLE GmbH, Developers' Version of TURBOMOLE V7.7.1, A Development of University of Karlsruhe and Forschungszentrum Karlsruhe GmbH, 1989–2007, TURBOMOLE GmbH, since 2007; available from https://www.turbomole.org (retrieved July 26, 2023).
[134]M. Häser, R. Ahlrichs, H. P. Baron, P. Weis, and H. Horn, Theor. Chim. Acta **83**, 455 (1992).
[135]C. van Wüllen and C. Michauk, J. Chem. Phys. **123**, 204113 (2005).
[136]CODATA Internationally Recommened 2018 Values of the Fundamental Physical Constans, https://physics.nist.gov/cuu/Constants/index.html (retrieved December 28, 2020).
[137]M. Sierka, A. Hogekamp, and R. Ahlrichs, J. Chem. Phys. **118**, 9136 (2003).
[138]F. Weigend, M. Kattannek, and R. Ahlrichs, J. Chem. Phys. **130**, 164106 (2009).
[139]M. K. Armbruster, F. Weigend, C. van Wüllen, and W. Klopper, Phys. Chem. Chem. Phys. **10**, 1748 (2008).
[140]U. Ekström, L. Visscher, R. Bast, A. J. Thorvaldsen, and K. Ruud, J. Chem. Theory Comput. **6**, 1971 (2010).
[141]M. A. L. Marques, M. J. T. Oliveira, and T. Burnus, Comput. Phys. Commun. **183**, 2272 (2012).
[142]S. Lehtola, C. Steigemann, M. J. T. Oliveira, and M. A. L. Marques, SoftwareX **7**, 1 (2018).
[143]Libxc, Version 6.2.2, available from https://www.tddft.org/programs/libxc/ (retrieved July 26, 2023).
[144]A. Klamt and G. Schüürmann, J. Chem. Soc., Perkin Trans. 2 **1993**, 799.
[145]A. Schäfer, A. Klamt, D. Sattel, J. C. W. Lohrenz, and F. Eckert, Phys. Chem. Chem. Phys. **2**, 2187 (2000).
[146]OpenMP Architecture Review Boards, OpenMP API Shared-Memory Parallel Programming, https://www.openmp.org (retrieved December 5, 2022).
[147]C. Holzer and Y. J. Franzke, OpenMP version of ridft, rdgrad, and egrad with contributions to mpshift, dscf, and grad; improved OpenMP version of aoforce and escf, released with TURBOMOLE V7.4 and further improved in TURBOMOLE V7.5, see https://www.turbomole.org/turbomole/release-notes-turbomole-7-5/ (retrieved July 31, 2023).
[148]P. von Ragué Schleyer, C. Maerker, A. Dransfeld, H. Jiao, and N. J. R. van Eikema Hommes, J. Am. Chem. Soc. **118**, 6317 (1996).
[149]P. R. von Schleyer and H. Jiao, Pure Appl. Chem. **68**, 209 (1996).
[150]R. Gershoni-Poranne and A. Stanger, Chem. Soc. Rev. **44**, 6597 (2015).
[151]D. Sundholm, H. Fliegl, and R. J. F. Berger, Wiley Interdiscip. Rev.: Comput. Mol. Sci. **6**, 639 (2016).
[152]P. Lazzeretti, Prog. Nucl. Magn. Reson. Spectrosc. **36**, 1 (2000).
[153]J. A. N. F. Gomes and R. B. Mallion, Chem. Rev. **101**, 1349 (2001).
[154]E. Steiner, P. W. Fowler, A. Soncini, and L. W. Jenneskens, Faraday Discuss. **135**, 309 (2007).
[155]K. P. Huber and G. H. Herzberg, *Constants of Diatomic Molecules* (Van Nostrand Reinhold, New York, 1979), see also https://webbook.nist.gov/ (retrieved August 1, 2023).
[156]J. Styszyński, Chem. Phys. Lett. **317**, 351 (2000).
[157]T. H. Dunning, J. Chem. Phys. **90**, 1007 (1989).
[158]R. A. Kendall, T. H. Dunning, and R. J. Harrison, J. Chem. Phys. **96**, 6796 (1992).
[159]K. G. Dyall, Theor. Chem. Acc. **115**, 441 (2006).
[160]Basis sets available from the Dirac program web site, http://dirac.chem.sdu.dk (retrieved March 26, 2020).
[161]P. A. M. Dirac, Proc. R. Soc. London, Ser. A **123**, 714 (1929).
[162]J. C. Slater, Phys. Rev. **81**, 385 (1951).
[163]S. H. Vosko, L. Wilk, and M. Nusair, Can. J. Phys. **58**, 1200 (1980).
[164]A. D. Becke, Phys. Rev. A **38**, 3098 (1988).
[165]J. P. Perdew, Phys. Rev. B **33**, 8822 (1986).
[166]A. D. Becke, J. Chem. Phys. **98**, 5648 (1993).
[167]C. Lee, W. Yang, and R. G. Parr, Phys. Rev. B **37**, 785 (1988).
[168]P. J. Stephens, F. J. Devlin, C. F. Chabalowski, and M. J. Frisch, J. Phys. Chem. **98**, 11623 (1994).
[169]J. P. Perdew and K. Schmidt, AIP Conf. Proc. **577**, 1 (2001).
[170]O. Treutler, "Entwicklung und Anwendung von Dichtefunktionalmethoden," Dr. rer. nat. dissertation (University of Karlsruhe (TH), Germany, 1995).
[171]O. Treutler and R. Ahlrichs, J. Chem. Phys. **102**, 346 (1995).
[172]Y. J. Franzke, R. Treß, T. M. Pazdera, and F. Weigend, Phys. Chem. Chem. Phys. **21**, 16658 (2019).
[173]T. Saue, R. Bast, A. S. P. Gomes, H. J. A. Jensen, L. Visscher, I. A. Aucar, R. Di Remigio, K. G. Dyall, E. Eliav, E. Fasshauer, T. Fleig, L. Halbert, E. D. Hedegård, B. Helmich-Paris, M. Iliaš, C. R. Jacob, S. Knecht, J. K. Laerdahl, M. L. Vidal, M. K. Nayak, M. Olejniczak, J. M. H. Olsen, M. Pernpointner, B. Senjean, A. Shee, A. Sunaga, and J. N. P. van Stralen, J. Chem. Phys. **152**, 204104 (2020).
[174]Manual of DIRAC Release 17, for DFT see https://diracprogram.org/doc/release-17/manual/dftcfun.html (retrieved August 3, 2023).
[175]T. W. Keal and D. J. Tozer, J. Chem. Phys. **119**, 3015 (2003).
[176]A. Bagno, G. Casella, and G. Saielli, J. Chem. Theory Comput. **2**, 37 (2006).
[177]J. P. Perdew, K. Burke, and M. Ernzerhof, Phys. Rev. Lett. **77**, 3865 (1996).
[178]C. Adamo and V. Barone, J. Chem. Phys. **110**, 6158 (1999).
[179]P. Pollak and F. Weigend, J. Chem. Theory Comput. **13**, 3696 (2017).
[180]TURBOMOLE GmbH, Manual of TURBOMOLE V7.7.1, A Development of University of Karlsruhe and Forschungszentrum Karlsruhe GmbH, 1989–2007, TURBOMOLE GmbH, since 2007; available from https://www.turbomole.org/turbomole/turbomole-documentation/ (retrieved July 26, 2023).
[181]F. Krätschmer, X. Sun, S. Gillhuber, H. Kucher, Y. J. Franzke, F. Weigend, and P. Roesky, Chem. Eur. J. **29**, e202203583 (2023).
[182]M. Balmer, Y. J. Franzke, F. Weigend, and C. von Hänisch, Chem. Eur. J. **26**, 192 (2020).
[183]V. N. Staroverov, G. E. Scuseria, J. Tao, and J. P. Perdew, J. Chem. Phys. **119**, 12129 (2003).
[184]T. Yanai, D. P. Tew, and N. C. Handy, Chem. Phys. Lett. **393**, 51 (2004).

[185]E. Caldeweyher, S. Ehlert, A. Hansen, H. Neugebauer, S. Spicher, C. Bannwarth, and S. Grimme, J. Chem. Phys. **150**, 154122 (2019).
[186]X.-W. Li, W. T. Pennington, and G. H. Robinson, J. Am. Chem. Soc. **117**, 7578 (1995).
[187]X.-W. Li, Y. Xie, P. R. Schreiner, K. D. Gripper, R. C. Crittendon, C. F. Campana, H. F. Schaefer, and G. H. Robinson, Organometallics **15**, 3798 (1996).
[188]R. J. Wright, M. Brynda, and P. P. Power, Angew. Chem., Int. Ed. **45**, 5953 (2006).
[189]X. Li, A. E. Kuznetsov, H.-F. Zhang, A. I. Boldyrev, and L.-S. Wang, Science **291**, 859 (2001).
[190]A. E. Kuznetsov, A. I. Boldyrev, X. Li, and L.-S. Wang, J. Am. Chem. Soc. **123**, 8825 (2001).
[191]B. Twamley and P. Power, Angew. Chem., Int. Ed. **39**, 3500 (2000).
[192]L. Yong, S. D. Hoffmann, T. F. Fässler, S. Riedel, and M. Kaupp, Angew. Chem., Int. Ed. **44**, 2092 (2005).
[193]M. Gausa, R. Kaschner, H. Lutz, G. Seifert, and K.-H. Meiwes-Broer, Chem. Phys. Lett. **230**, 99 (1994).
[194]A. R. Eulenstein, Y. J. Franzke, N. Lichtenberger, R. J. Wilson, H. L. Deubner, F. Kraus, R. Clérac, F. Weigend, and S. Dehnen, Nat. Chem. **13**, 149 (2021).
[195]B. Peerless, A. Schmidt, Y. J. Franzke, and S. Dehnen, Nat. Chem. **15**, 347 (2023).
[196]J. Vícha, J. Novotný, M. Straka, M. Repisky, K. Ruud, S. Komorovsky, and R. Marek, Phys. Chem. Chem. Phys. **17**, 24944 (2015).
[197]W. McFarlane, J. Chem. Soc. A **1968**, 1630.
[198]T. N. Mitchell, A. Amamria, B. Fabisch, H. G. Kuivila, T. J. Karol, and K. Swami, J. Organomet. Chem. **259**, 157 (1983).
[199]T. Birchall and A. Pereira, J. Chem. Soc., Chem. Commun. **1972**, 1150.
[200]W. L. Jolly and J. R. Webster, Inorg. Chem. **10**, 877 (1971).
[201]J. B. Lambert, Y. Zhao, H. W. Wu, W. C. Tse, and B. Kuhlmann, J. Am. Chem. Soc. **121**, 5001 (1999).
[202]E. V. Van Den Berghe and G. P. Van Der Kelen, J. Organomet. Chem. **26**, 207 (1971).
[203]C. R. Lassigne and E. J. Wells, Can. J. Chem. **55**, 927 (1977).
[204]J. J. Burke and P. C. Lauterbur, J. Am. Chem. Soc. **83**, 326 (1961).
[205]W. McFarlane and R. J. Wood, J. Organomet. Chem. **40**, C17 (1972).
[206]J. D. Kennedy, W. McFarlane, G. S. Pyne, P. L. Clarke, and J. L. Wardell, J. Chem. Soc., Perkin Trans. 2 **1975**, 1234.
[207]J. Jaramillo, G. E. Scuseria, and M. Ernzerhof, J. Chem. Phys. **118**, 1068 (2003).
[208]C. Holzer and Y. J. Franzke, J. Chem. Phys. **157**, 034108 (2022).
[209]Y. J. Franzke, L. Spiske, P. Pollak, and F. Weigend, J. Chem. Theory Comput. **16**, 5658 (2020).
[210]S. Gillhuber, Y. J. Franzke, and F. Weigend, J. Phys. Chem. A **125**, 9707 (2021).
[211]C. J. Jameson, A. De Dios, and A. Keith Jameson, Chem. Phys. Lett. **167**, 575 (1990).
[212]P. v. R. Schleyer, Chem. Rev. **101**, 1115 (2001).
[213]E. Hückel, Z. Phys. **70**, 204 (1931).
[214]E. Hückel, Z. Phys. **72**, 310 (1931).
[215]E. Hückel, Z. Phys. **76**, 628 (1932).
[216]*IUPAC, Compendium of Chemical Terminology (The Gold Book)*, 2nd ed., edited by A. D. McNaught and A. Wilkinson (Blackwell Scientific Publications, Oxford, United Kingdom, 1997), xML on-line corrected version: http://goldbook.iupac.org (2006), created by M. Nic, J. Jirat, and B. Kosata; updates compiled by A. Jenkins, For Hückel's rule see https://goldbook.iupac.org/H02867.html (retrieved July 30, 2023).
[217]L. Pauling, J. Chem. Phys. **4**, 673 (1936).
[218]J. Jusélius, D. Sundholm, and J. Gauss, J. Chem. Phys. **121**, 3952 (2004).
[219]H. Fliegl, S. Taubert, O. Lehtonen, and D. Sundholm, Phys. Chem. Chem. Phys. **13**, 20500 (2011).
[220]D. Sundholm, M. Dimitrova, and R. J. F. Berger, Chem. Commun. **57**, 12362 (2021).
[221]GIMIC, Version 2.1.4 (merge 3a5f0eb, 2019), available from https://github.com/qmcurrents/gimic (retrieved November 26, 2020).
[222]R. J. F. Berger and M. Dimitrova, Phys. Chem. Chem. Phys. **24**, 23089 (2022).
[223]R. J. F. Berger, M. Dimitrova, R. T. Nasibullin, R. R. Valiev, and D. Sundholm, Phys. Chem. Chem. Phys. **24**, 624 (2022).
[224]D. Sulzer, M. Olejniczak, R. Bast, and T. Saue, Phys. Chem. Chem. Phys. **13**, 20682 (2011).
[225]R. J. F. Berger, M. Repisky, and S. Komorovsky, Chem. Commun. **51**, 13961 (2015).
[226]L. Alvarez-Thon and W. Caimanque-Aguilar, Chem. Phys. Lett. **671**, 118 (2017).
[227]F. Jensen, J. Chem. Theory Comput. **4**, 719 (2008).
[228]F. Jensen, J. Chem. Theory Comput. **11**, 132 (2015).
[229]M. K. Armbruster, W. Klopper, and F. Weigend, Phys. Chem. Chem. Phys. **8**, 4862 (2006).
[230]A. Pausch and C. Holzer, J. Phys. Chem. Lett. **13**, 4335 (2022).
[231]C. C. J. Roothaan, Rev. Mod. Phys. **23**, 69 (1951).
[232]G. G. Hall, Proc. R. Soc. London, Ser. A **205**, 541 (1951).